2013

Mechanical stability and internal friction of GB1 protein

WEI ZHANG
Lehigh University

Mechanical stability and internal friction of GB1 protein

by

Wei Zhang

Presented to the Graduate and Research Committee

of Lehigh University

in Candidacy for the Degree of

Master of Science

in

Mechanical Engineering and Mechanics

Lehigh University

September, 2013

This thesis is accepted and approved in partial fulfillment of the requirements for the Master of Science.

_____

Date

_____

Xiaohui (Frank) Zhang

_____

D. Gary Harlow, Chairperson

Department of Mechanical Engineering and Mechanics

Acknowledgements

I would like to express my since gratitude to Dr. Xiaohui (Frank) Zhang for his guidance, teaching and support throughout this work. He provided me not only with the opportunity, but also the skills needed to apply some of the most advanced techniques to the cutting edge field of molecular bioengineering. And, without his knowledge and kindness I would not be able to write this dissertation. I also want to thank the postdoc Yizhen Wang and all other members in Frank's laboratory for the help that they provided in helping me complete this dissertation. Yizhen created the initial idea for the concept behind my thesis, and helped me with the experiments and data analysis. I would also like to thank Chenyu Wu for helping me with the biological aspects of the project, an area which I have had little background in before I started this project. Meanwhile, I want to express my sincere thanks to Dr. Hongbin Li for providing us the $(GB1)_8$ plasmid and protocol for protein purification, and for discussing experimental results with us.

I want to thank department of Mechanical Engineering and Mechanics and the MEM graduation program for providing me with the financial support and creative research environment. I also want to express my sincere gratitude to Dr. Gary Harlow and Dr. Donald Rockwell for their help and support.

At last, I would like to thank my parents for supporting my career decisions and giving their unconditional love to me.

Table of Contents

List of Tables

List of Figures

Abstract

Internal friction plays an important role in protein dynamics by modulating the protein's folding/unfolding process and other conformational changes. However, how to quantify internal friction and its contribution to protein folding/unfolding dynamics remains challenging. Single-molecule force spectroscopy has developed as a powerful tool to probe protein structure and dynamics. In this thesis, with the technique of atomic force microscopy (AFM), we measured the single-molecule force spectroscopy of the GB1 protein's unfolding process. By changing the solvent viscosity and the concentrations of denaturant GdmCl, we were able to extract the key mechanical properties, such as the spontaneous unfolding rate k_0, the intrinsic lifetime τ_0, the location of the activation state $\Delta x^{\ddagger}$, and the height of activation energy ΔG, according to both Bell-Evans model and Dudko's model. Moreover, we developed an extended Ansari-expression to describe the relation between the overall friction and internal friction. By fitting the extracted mechanical properties to the expression, we successfully quantified the internal friction, which decreases from ~ 2.1 mPa s without any denaturant to ~ 1.0 mPa s with 2M denaturant GdmCl. The single-molecule procedure provided a unique way to quantify internal friction in protein's folding/unfolding process.

Chapter 1

Introduction

In biology one hot topic that has a strong connection with human's life, is protein folding and conformational change. The conformational change is said to be driven by thermal fluctuations (Kramers in 1940 [1]). The theory considers the protein process as a diffusive process, with a classical particle of mass M moves in a one-dimensional asymmetric double-well potential $U(x)$ (Figure 2.1). In this simplified two-state model, all the reacting and solvent molecules constitute a heat bath at temperature T. Kramers deduced the celebrated relation between the rate of escape (i.e., unfolding/unfolding rates) between the environment parameters, including the friction, the free activation energy, and the system absolute temperature, at both large solvent viscosity limit and small viscosity limit. Though the theory was successfully built, it was not until about thirty years later that the theory was applied to analyze the experimental results due to the unavailability of experimental techniques.

Based on the widely accepted Kramers theory at large solvent viscosity limit, two models were built to further extract the mechanical properties of single molecules; the Bell-Evans model and Dudko's model.

The Bell-Evans model was first proposed by Bell to describe the rate of bond dissociation under external force load phenomenologically [2], and later refined by Evans by deriving the dependence of strength of adhesion (the most probably rupture force) on the force loading rate

[3]. This powerful model is used to extract the reaction kinetics in liquids to bond dissociation under an external force, with a given distribution of rupture forces and the corresponding force loading rate. The extracted mechanical properties include the intrinsic rate coefficient/lifetime (k_0/τ_0), as well as the distance between the low-energy native state and the high-energy transition state along the reaction coordinate $\Delta x^{\ddagger}$. It predicts that a linear relationship between the most probable unfolding/rupture forces F^* and the corresponding force loading rate $\dot{F}$ (Eq. (2.14)). However, the model fails to directly give the height of free activation energy for either the folding process (ΔG_f) or unfolding process (ΔG_u) of protein. Meanwhile, the model still can tell the free energy difference between the native state and the unfolded state, namely, $\Delta\Delta G = \Delta G_f - \Delta G_u$.

The other model for extracting kinetic information from single-molecule pulling experiments is proposed by Dudko *et al.* in 2006 [4]. By introducing a new free-energy surface factor ν, the model is able to include Bell's formula as a special case (with $\nu = 1$). Different from the Bell-Evans model, the unified Dudko's model provides estimates of the free energy of activation ΔG, as well as another two important mechanical parameters given in Bell-Evans model, i.e., the intrinsic rate coefficient/lifetime (k_0/τ_0) and the location of the transition state $\Delta x^{\ddagger}$. This model uses an analytical expression (Eq. (2.24)) to describe the relationship between the force-dependent rate of escape k and the applied force F, intrinsic rate coefficient k_0, location of the barrier $\Delta x^{\ddagger}$, and height of the barrier ΔG, with a free-energy surface factor ν, and predicts that the mean rupture force $\langle F \rangle \sim \ln(v)$, where v is the pulling speed. To get enough data of the force-dependent rate of escape ($k(F)$), we can either get the experiments done at different pulling speeds, or at a constant ramp-force. For the first one, the technique used is to transform rupture- or unfolding-force histograms into the force-dependent lifetimes (Eq. (2.32)), which can be directly obtained in the second one.

All these theories have been validated with the tool of single-molecule force spectroscopy. The most common force-spectroscopy techniques are atomic force microscopy (AFM), optical tweezers and magnetic tweezers. These advanced techniques make it possible for people to investigate the mechanical properties of an individual biological molecule, without the interference

from other molecules. The atomic force microscopy (AFM) is the simplest in concept, and most widely used among the three force-spectroscopy techniques. The AFM was the device chosen for our experiments. AFM has a large force range ($\sim$ 10 pN $-$ 10^4 pN), high force sensitivity ($\sim$ 10 pN/nm), as well as good spatial and temporal resolution (0.5 nm and 10^{-3} s).[5]

It is found that protecting osmolytes, such as glycerol and sarcosine, slow down the intrinsic unfolding rate of a globular protein while accelerate its folding rate concurrently, independent of the applied force and without any complexion at the transition state.[6] These results simply agree with the Kramers theory at a strong viscosity limit, due to the rate of escape (k) is positively correlated with the reciprocal of solvent viscosity ($1/\eta$), if we simply equal the friction γ in Kramers theory (Eq. (2.2)) to η. However, as more single-molecule experiments were carried out, deviations of rate coefficient (k) from simply $1/\eta$ were observed [7][8]. This caused us to revaluate our use of Kramers theory. The reason is that Kramers derived the expression by simplifying the reaction process to a simple one-dimensional diffusion process, while the rate of escape k deduced actually represents the overall rate, with an "effective" friction coefficient γ accounting for all the mechanisms that the energy can dissipate out during the reaction process. The friction coefficient γ, at least, includes the effects of both solvent dynamic friction η and the solvent-independent internal friction σ. Previous experiments has shown that the internal friction might play an important role in protein folding dynamics [9], and its contribution to protein unfolding dynamics has been quantified by determining the reconfiguration times of unfolded proteins through single-molecule spectroscopy recently [10]. Despite their great efforts, to directly quantify the internal friction and understand its contribution to protein folding/unfolding dynamics, much of the mechanisms behind it still remains unclear.

In this experiment, we used the atomic force microscopy (AFM) technique, combined with protein engineering, to investigate the mechanical stability of protein folding/unfolding. The protein we used is an artificial polyprotein $(GB1)_8$, a tandem repeat of eight identical units of elastomeric protein GB1. This project consists of two goals. **The first goal of our study** is to investigate the mechanical stability and energy landscape of GB1 protein, and identify the contri-

bution of solvent viscosity and denaturant. To realize this goal, we pulled the polyprotein $(GB1)_8$ at varied concentrations of glycerol and denaturant GdmCl, and setting different constant pulling speeds. Then we extracted the key mechanical properties according to both Bell-Evans model and Dudko's model, and compared their differences. Indeed, the mechanical and biophysical properties of the monomer GB1 were first reported in Chao Yi and Dr. Hongbin Li's seminal work.[11][12] **Our second goal** is to quantify the internal friction directly from the extracted kinetic parameters according to both models. To accomplish this, we developed an extended Ansari-expression to describe the relation between the overall friction and internal friction. By fitting the extracted mechanical properties to the expression, we successfully quantified the internal friction.

For the following chapters, Chapter 2 will introduce the theoretical basis for this project, including the Kramers theory, Bell-Evans model, Dudko's model, and worm-like chain model. Chapter 2 will also explain the experimental methodology including protein engineering, single molecule experiments etc.. In Chapter 3, we will show how to extract the mechanical properties of the unfolding process of GB1 protein, using both the Bell-Evans and Dudko's model, as well as how we figured out the unfolding energy landscape, and gave the contribution of solvent viscosity and denaturant. In Chapter 4, we will use the extended Ansari-expression developed to quantify the internal friction of GB1 unfolding dynamics. We will conclude the dissertation in Chapter 5 with our findings from the experiments.

Chapter 2

Theory and Experimental Methodology

2.1 Single-molecule kinetic mechanisms and models

Single-molecule pulling experiments are used to reveal the following kinetic properties: (1) the spontaneous dissociation rate or the intrinsic rate coefficient k_0; (2) the distance between the native state and the transition state along the reaction coordinate, namely the location of the transition state $\Delta x^{\ddagger}$; (3) the unfolding barrier or the free energy of activation ΔG.

2.1.1 Kramers theory

In Kramers theory [1][13], chemical reactions are treated as diffusion problems. Based on a derivation of the Fokker-Plank diffusion equation [14] for the Brownian motion in phase space, in the presence of a nonlinear potential field, Kramers predicted the probability of escape (usually called "rate of escape" now) k depending on the temperature T and the friction γ. In the model of chemical reactions, a classical particle of mass M moves in a one-dimensional asymmetric double-well potential $U(x)$ (shown in Figure 2.1). Along the reaction coordinate x, the particle has minima of potential at x_a and x_c, denoting the reactant and product states, respectively. The local maximum point at x_b separating these states corresponds to the transition state (or activated complex). In this simplified model, all the reacting and solvent molecules constitute a heat bath

at temperature T. The effect of temperature on the particle is described by a fluctuating force $\xi(t)$ and by a linear damping force $-M\gamma\dot{x}$, where γ is a constant damping rate from friction. Kramers distinguished two limiting regimes, one with strong friction (spatial-diffusion regime), and the other with a low damping rate (energy-diffusion regime).

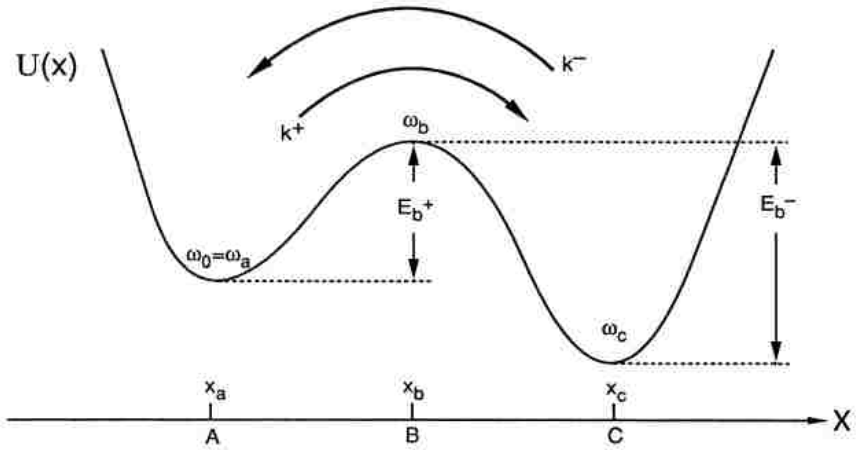

Figure 2.1: Asymmetric potential field $U(x)$ with two metastable states (this schematic diagram was adopted from [13]). There are two metastable wells at x_a and x_c, as well as a transition state at x_b along the reaction coordinate x. Escape occurs via the forward rate k^+, and the backward rate k^-, respectively. $E_b^{\pm}$ correspond to the activation energies. $\omega_a,\ \omega_b,\ \omega_c$ denote the angular frequency at each point, with parameter $\omega_0 = \omega_a$.

For solvent with strong friction γ (large viscosity), Kramers derives the celebrated result of the escape rate from A to C, $k_{A\to C}$

$$k_{A\to C} \equiv k^+ = \frac{(\gamma^2/4 + \omega_b^2)^{1/2} - \gamma/2}{\omega_b} \cdot \frac{\omega_0}{2\pi} \exp(-\beta E_b) \tag{2.1}$$

where $\omega_0 = \omega_a$, with ω_a and ω_b denote the angular frequency at x_a and x_b, respectively, $E_b = U(x_b) - U(x_a)$ is the activation energy, and thermal factor $\beta = (k_B T)^{-1}$.

In the limit of very large damping (the Smoluchowski limit), i.e., for $\gamma/2 \gg \omega_b$, using Taylor expansion for $(\gamma^2/4 + \omega_b^2)^{1/2} - \gamma/2$ leads to [1]

$$k_{A\to C} \equiv k^+ = \frac{\omega_0 \omega_b}{2\pi\gamma} \exp(-\beta E_b) \tag{2.2}$$

which shows that the rate of escape k decreases inversely proportional to the friction γ.

For very weak friction γ (small viscosity), it gives

$$k_{A\to C} \equiv k^{+} = \gamma\beta E_b \exp(-\beta E_b) \tag{2.3}$$

all the parameters are same as these in Eq. (2.1).

2.1.2 Bell-Evans model

In Chapter 2.1.1, Kramers has derived the analytical formula for the rate of escape, but it was not used until about thirty years later due to the unavailability of experimental techniques. Kramers presented the reaction kinetics in liquids.[1] By extending the kinetic theory of the strength of solids [15] and the transition state theory for reactions in gases introduced by Eyring and others [13], Bell first proposed the phenomenological model to describe the rate of bond dissociation under external force load in 1978 [2], while later Evans refined the theory by deriving the dependence of strength of adhesion (the most probably rupture force) on the loading rate [3].

The earliest theory concerning the reaction rate was developed by Arrhenius [16], given by the Van't Hoff-Arrhenius law: rate of dissociation $k = \nu \exp(-\frac{E_0}{k_B T})$, where v is the natural frequency of molecular collisions in the collision theory in vacuum, E_0 is the free entropy term in the transition state theory, k_B is Boltzmann constant, and T is the absolute temperature.

The universal rate relation between lifetime τ, stress F, and the absolute temperature T in solid mechanics was derived by Zhurkov [15], which was introduced to analyze the lifetime of molecular bonds by Bell [2]

$$\tau = \tau_0 \exp(\frac{E_0 - \gamma F}{k_B T}) \tag{2.4}$$

where k_B is Boltzman constant, τ_0 is the reciprocal of natural frequency of oscillation of atoms in solids, E_0 is the bond energy, and γ is a parameter determined empirically. As applied to receptor-ligand bonds, the formula predicts that the bonds' lifetime is calculated at $F = 0$. These

results can also been derived directly from Kramers theory in the strong friction case with Eq. (2.1).

Assuming that the applied external force F acts directly along the reaction coordinate, i.e., the height of the transition-state energy barrier depends linearly on the applied force F and a constant distance $\Delta x^{\ddagger}$ between the native equilibrium state and the transition state, Evans *et al.* got the force-dependent dissociation rate [3]:

$$k(F) = \frac{\omega_{min}\omega_{max}}{2\pi\gamma} \exp(-\frac{E_0 - F\Delta x^{\ddagger}}{k_B T}) = k_0 \cdot \exp(\frac{F\Delta x^{\ddagger}}{k_B T}) = k_0 \cdot \exp(\beta F \Delta x^{\ddagger}) \tag{2.5}$$

where ω_{min} represents the angular frequency of the metastable state, ω_{max} is the positive valued angular frequency of the transition state at the barrier, γ is the damping relaxation rate, k_0 is the zero-force natural off rate, k_B is Boltzmann constant, T is the absolute temperature, and $\beta = (k_B T)^{-1}$.

The force-dependent lifetime $\tau(F)$ is the reciprocal of the force-dependent dissociation rate $k(F)$, i.e.,

$$\tau(F) = \tau_0 \exp(-\beta F \Delta x^{\ddagger}) \tag{2.6}$$

Here $\tau_0 = k_0^{-1}$ is the intrinsic lifetime, the lifetime under no applied force.

The rate of dissociation k can be used to describe the change of existing bonds N_B with time t,

$$\frac{\mathrm{d}N_B(t)}{\mathrm{d}t} = -k \cdot N_B(t) \tag{2.7}$$

The number of intact bonds $N_B(t)$ is given be integrating Eq. (2.7)

$$N_B(t) = \exp\left(-\int_0^t k(t')\mathrm{d}t'\right) \tag{2.8}$$

Assuming that the force F is a reversible continuous function of time t, t can be replaced by F,

which results in the following expression:

$$N_B(t) = \exp\left(-\int_0^F k(f)\cdot\frac{1}{\dot{f}}\mathrm{d}f\right) \tag{2.9}$$

Then the number of dissociated bonds N_D at time t is given by

$$N_D(t) = 1 - N_B(t) = 1 - \exp\left(-\int_0^F k(f)\cdot\frac{1}{\dot{f}}\mathrm{d}f\right) \tag{2.10}$$

The probability $p(F)$ that the bond breaks under external stress F is given by $\frac{\mathrm{d}N_D}{\mathrm{d}F}$:

$$p(F) = \frac{\mathrm{d}N_D}{\mathrm{d}F}(F) = \frac{k(F)}{\dot{F}(F)}\cdot\exp(-\int_0^F \frac{k(f)}{\dot{F}(f)}\,\mathrm{d}f) \tag{2.11}$$

where $\dot{F}(F) = \mathrm{d}F/\mathrm{d}t$ is the force loading rate [2]. It can be demonstrated that $\int_0^\infty p(F)\mathrm{d}F = 1$.

For Bell-Evans model, using Eq. (2.5) leads to

$$p(F)_{B-E-k-f} = \frac{k_0}{\dot{F}}\exp(\beta F\Delta x^\ddagger)\cdot\exp(-k_0\int_0^F\frac{1}{\dot{F}}\exp(\beta F\Delta x^\ddagger)) \tag{2.12}$$

Thus, the most probable rupture force F^* can be found by derivation:

$$\left.\frac{\mathrm{d}p(F)}{\mathrm{d}F}\right|_{F=F^*} = 0 \tag{2.13}$$

Assuming that the loading rate $\dot{F}$ is independent of the applied force F, like these in constant speed experiments, we can get a linear dependence of F^* on the logarithm of the loading rate $\dot{F}$:

$$F^*(\dot{F}) = \frac{1}{\beta\Delta x^\ddagger}\ln(\frac{\beta\Delta x^\ddagger}{k_0}\dot{F}) = \frac{1}{\beta\Delta x^\ddagger}\ln(\dot{F}) + \frac{1}{\beta\Delta x^\ddagger}\ln(\frac{\beta\Delta x^\ddagger}{k_0}) \tag{2.14}$$

According to Eq. (2.14), we can extract the single molecule kinetic information, i.e., the natural dissociation rate k_0 and the location of the transition state $\Delta x^\ddagger$, given the distribution of the

rupture forces and the corresponding loading rates. That is

$$\begin{aligned} \Delta x^{\ddagger} &= \frac{k_B T}{m} \\ k_0 &= \frac{1}{m} \exp(-\frac{b}{m}) \end{aligned} \tag{2.15}$$

where m and b signify the slope and the y-intercept of the best fit straight line (x-axis: $\ln \dot{F}$, y-axis: F^*).

If flexible linkers are used in the pulling experiments, the force loading rate under investigation is changing continuously when stretching the molecule. In this case, the assumption that $\dot{F}$ is independent of F is not fulfilled, and Eq. (2.14) is only an approximate description.

It is also reported that the mean force $\overline{F}$ and median force F_m of the distribution can be used to extracted the kinetic parameters $\Delta x^{\ddagger}$ and k_0 [17][18], with

$$\begin{aligned} \overline{F} &= \int_0^{\infty} F p(F) \, \mathrm{d}F \\ S(F)|_{F=F_m} &= \frac{1}{2} \end{aligned} \tag{2.16}$$

2.1.3 Dudko model

Based on the Kramers theory and certain scaling laws obtained by Garg [19] for high forces, Dudko *et al.* [4] built a unified framework for extracting mechanical properties from single-molecule pulling experiments.

Exerted an external pulling force F, the molecule moves on a combined free-energy surface, with potential

$$U(x) = U_0(x) - Fx \tag{2.17}$$

where x is the position change along the pulling direction, and $U_0(x)$ is the free energy in the absence of external force. In single-well model, $U_0(x)$ has a lowest single well at $x = 0$, and a barrier at $x = \Delta x^{\ddagger}$ of height ΔG. Under an external force F, the barrier height $\Delta U(F)$ decreases, shown in Figure 2.2.

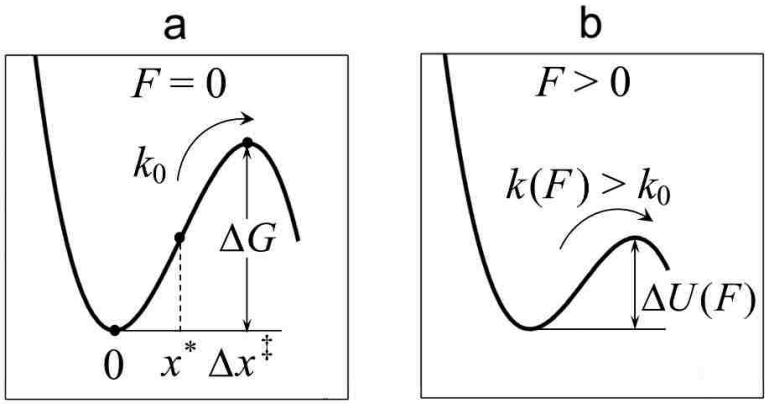

Figure 2.2: Force effect on a single-well free-energy surface (this schematic diagram was adopted from [4]). (a) Intrinsic free-energy surface $U_0(x)$ with barrier width $\Delta x^{\ddagger}$ between the native state and the transition state along the reaction coordinate, activation free energy ΔG, and inflection point x^*; (b) decrease of the activation energy $\Delta U(F)$ of the combined free-energy surface, $U(x) = U_0(x) - Fx$, due to the presence of an external force F, and the reaction rate $k(F)$ also increases (larger than spontaneous reaction rate k_0).

For single-molecule experiments at constant force or constant pulling speed, the unfolding process is stochastic. Under an adiabatic approximation, the survival probability $S(t)$ that the system keeps intact at time t satisfies the first-order rate equation $\dot{S}(t) \equiv dS/dt = -S(t)/\tau(F(t))$, ignoring fluctuations in the time-dependent external force $F(t)$ [20]. Also, $-\dot{F}(t)dt = p(F)dF$, then the rupture forces have a probability density distribution [19][21] (same as Eq. (2.11)):

$$p(F) = -\frac{\mathrm{d}S(F)}{\mathrm{d}F} = \frac{k(F)}{\dot{F}(F)} \cdot \exp(-\int_0^F \frac{k(f)}{\dot{F}(f)}\,\mathrm{d}f)$$

Here, $S(F)$ is the bond survival probability that the molecular system keeps intact at time t, $\dot{F}(F) = \mathrm{d}F/\mathrm{d}t$ is the force loading rate at force F, and $k(F) = \tau(F)^{-1}$ is the force-dependent dissociation rate, where $\tau(F)$ is the lifetime.[2] It can be demonstrated that $\int_0^\infty p(F)\mathrm{d}F = 1$.

The mean rupture force and its variance then can be represented by

$$\langle F \rangle = \int_0^\infty F \cdot p(F)\mathrm{d}F \qquad\qquad \sigma_F^2 = \langle F^2 \rangle - \langle F \rangle^2 \tag{2.18}$$

The dissociation rate $k(F)$

The dissociation rate in Dudko's model is specifically calculated from Kramers theory describing the escape over a one-dimensional, single-well potential field.[1] For a sufficiently high potential barrier, the force-dependent rate of escape is predicted as:

$$k/k_0 = [\int_{well} e^{-U(x)}\mathrm{d}x \int_{barrier} e^{U(x)}\mathrm{d}x]^{-1} \cdot [\int_{well} e^{-U_0(x)}\mathrm{d}x \int_{barrier} e^{U_0(x)}\mathrm{d}x] \tag{2.19}$$

For constant pulling speed, the external pulling force is $F(t) = K \cdot vt$, where K is the spring constant for the stiff molecular system; the combined free-energy surface is given by $U(x) = U_0(x) + K(x - vt)^2/2$. For a soft effective spring, $K \ll 2\Delta G/\Delta x^{\ddagger 2}$, using first-order Taylor series expansion, it implies

$$U(x) \approx U_0(x) - Kvtx = U_0(x) - Fx \tag{2.20}$$

Substitution Eq. (2.20) back to Eq. (2.19), get

$$k/k_0 = [\int_{well} e^{-U_0(x)+Fx}\mathrm{d}x \int_{barrier} e^{U_0(x)-Fx}\mathrm{d}x]^{-1} \cdot [\int_{well} e^{-U_0(x)}\mathrm{d}x \int_{barrier} e^{U_0(x)}\mathrm{d}x] \tag{2.21}$$

To get an analytical formulation for k, two kinds of sing-well model with free-energy surfaces $U_0(x)$ for external forces, which grow linearly with time, are considered:
The cusp surface [20]:

$$U_0(x) = \Delta G(x/\Delta x^{\ddagger})^2 \quad for\ x < \Delta x^{\ddagger},\ and\ -\infty \quad for\ x \geq \Delta x^{\ddagger} \tag{2.22}$$

The linear-cubic surface:

$$U_0(x) = \frac{3}{2}\Delta G(x/\Delta x^{\ddagger}) - 2\Delta G(x/\Delta x^{\ddagger})^3 \tag{2.23}$$

The force-dependent dissociation rate $k(F)$ can be derived in a unified form [4]:

$$k(F) = k_0(1 - \frac{\nu F \Delta x^{\ddagger}}{\Delta G})^{1/\nu - 1} \cdot \exp\{\beta \Delta G[1 - (1 - \frac{\nu F \Delta x^{\ddagger}}{\Delta G})^{1/\nu}]\} \tag{2.24}$$

In this expression, k_0, $\Delta x^{\ddagger}$, and ΔG are the three most important kinetic parameters, the intrinsic dissociation rate, the distance between the native state and the transition state along the reaction coordinate, and the apparent free energy of activation in the absence of an external force. ν is a scaling factor, which specifies different kinds of free-energy surface profile. For $\nu = 1/2$, formula (2.24) corresponds to the cusp surface described by Eq. (2.22), either a harmonic well or barrier; for $\nu = 2/3$, formula (2.24) corresponds to the linear-cubic surface described by Eq. (2.23); for $\nu = 1$, formula (2.24) recovers to the Bell-Evans' formula, exactly same as Eq. (2.5), which means that the Bell-Evans model is a special case of Dudko model.

The lifetime $\tau(F) = k(F)^{-1}$, substituting to Eq. (2.24) leads to

$$\tau(F) = \tau_0(1 - \frac{\nu F \Delta x^{\ddagger}}{\Delta G})^{1 - 1/\nu} \cdot \exp\{-\beta \Delta G[1 - (1 - \frac{\nu F \Delta x^{\ddagger}}{\Delta G})^{1/\nu}]\} \tag{2.25}$$

If ΔG is calculated in unit of $k_B T$, expression (2.25) changes to

$$\tau(F) = \tau_0(1 - \frac{\nu \beta F \Delta x^{\ddagger}}{\Delta G})^{1 - 1/\nu} \cdot \exp\{-\Delta G[1 - (1 - \frac{\nu \beta F \Delta x^{\ddagger}}{\Delta G})^{1/\nu}]\} \tag{2.26}$$

The loading rate $\dot{F}$

If the link effect is neglected, the loading rate $\dot{F} = dF/dt = Kv$, which is independent of F. But for experimental setup with intervening flexible linkers, like DNA handles, the loading rate is a function of applied force, i.e., $\dot{F} = \dot{F}(F)$. Considering the pulling process as a simple force-balance process, the force-dependent loading rate $\dot{F}(F)$ is given by [22]

$$\frac{1}{\dot{F}(F)} = \frac{1}{vK} + \frac{1}{v}\frac{\mathrm{d}l(F)}{\mathrm{d}F} \tag{2.27}$$

where v is the pulling velocity, K is the spring constant of cantilever in AFM experiments, $l(F)$ is the force-dependent extension of the linker.

For the worm-like chain (WLC) model, the extension $l(F)$ of the flexible linker is approximately the solution of Eq. (2.28) (discussed in Chapter 2.1.4)

$$\frac{F \cdot L_p}{k_B T} = \frac{1}{4}\left(1 - \frac{l(F)}{L_c}\right)^{-2} - \frac{1}{4} + \frac{l(F)}{L_c} \tag{2.28}$$

where F is the applied force, L_c is the contour length, L_p is the persistence length of the WLC linker, k_B is Boltzmann constant, and T is the absolute temperature. By taking into account the first two terms in the low-force expansion of $\mathrm{d}l/\mathrm{d}F$ with the limit $F \to \infty$, an approximate analytical Padé-like expression for the force-dependent loading rate $\dot{F}$ is given by [23]

$$\dot{F}(F) = v\left[\frac{1}{K} + \frac{2\beta L_c L_p(1+\beta F L_p)}{3 + 5\beta F L_p + 8(\beta F L_p)^{5/2}}\right]^{-1} \tag{2.29}$$

We can see that the second factor in the right hand side accounts for the link effect. If we ignore this part, the expression turns to the simple one $\dot{F} = Kv$. It is said that this expression is accurate to within $\sim 3.5\%$ [23].

For the analogous expression for a freely jointed chain (FJC), the force-dependent loading rate $\dot{F}$ is given by Ray *et al.* [22]

$$\dot{F}(F) = Kv\left\{1 + \frac{KL_c}{F_K}\left[(\frac{F_K}{F})^2 - \mathrm{csch}^2(\frac{F}{F_K})\right]\right\}^{-1} \tag{2.30}$$

where L_c is the contour length of the linker, K is the cantilever spring constant in AFM experiments, and the parameter $F_K = k_B T/a$ where a is the Kuhn length of the linker. It is also true that the loading rate approaches Kv under conditions of high force F, short linker L_c, or small spring constant K.

Data analysis

For constant pulling speed and constant force experiments, in Eq. (2.24), (2.25) and (2.26), k_0 (or τ_0), $\Delta x^{\ddagger}$, and ΔG are unknown parameters, which need to be fitted from the experimental data; $k(F)$ (or $\tau(F)$) and F are extracted directly from the experimental results; β and the scaling factor ν are known constant.

Based on Eq. (2.1.3), under the quasi-adiabatic approximation, the transformation from constant speed experiments to constant force experiments is given by [4][23][24]

$$\tau(F) = \frac{\int_F^{\infty} p(f|v)\mathrm{d}f}{\dot{F}(F|v) \cdot p(F|v)} \tag{2.31}$$

In this expression, $p(F|v)$ is the rupture-force probability density distribution measured at constant pulling speed v, $\tau(F)$ is the lifetime at constant force F, and $\dot{F}(F|v)$ is the loading rate at speed v. This transformation is applicable to all kinds of underlying free-energy surface. For each pulling speed v (or loading rate $\dot{F}(F)$), a set of $(F, \tau(F))$ pairs are obtained according to Eq. (2.31), and it is predicted that different sets of $(F, \tau(F))$, from different v, should collapse onto one single master curve over a wide range of rupture forces.

Consider an experimental rupture-force histogram obtained at constant speed v, the histogram has N bins of width $\Delta F = (F_{max} - F_{min})/N$. Let the number of counts in the ith bin be c_i, $1 \leq i \leq N$, then the total counts is $C = \sum_{i=1}^{N} c_i$, resulting in the probability $P(F_i) = c_i/C$, and the density $p(F_i) = c_i/(C \cdot \Delta F)$. Thus, substituting to Eq. (2.31)

$$\tau(F_i) = \frac{\left(p(F_i)/2 + \sum_{k=i+1}^{N} p(F_i)\right) \cdot \Delta F}{\dot{F}(F_i) \cdot p(F_i)} \tag{2.32}$$

where $F_i = F_{min} + (i - 1/2)\Delta F$, for $1 \leq i \leq N-1$; $\tau(F_N) = \frac{p(F_N)/2 \cdot \Delta F}{\dot{F}(F_N) \cdot p(F_N)} = \frac{\Delta F}{2\dot{F}(F_N)}$, for $i = N$.

A quite general approximation of the relationship between the lifetime at the mean rupture

force and the variance of the rupture-force distribution is given by [23]

$$\tau(\langle F\rangle) \approx \left[\frac{\pi}{2}(\langle F^2\rangle - \langle F\rangle^2)\right]^{1/2} / \dot{F}(\langle F\rangle) \tag{2.33}$$

This expression is derived from Eq. (2.31) by approximating the rupture-force distribution $p(F)$ to be a normalized Gaussian distribution, and setting the rupture force $F = \langle F\rangle$. Actually, the real rupture-force distribution is not well described by the Gaussian distribution over the entire range of rupture forces, but the approximation of the lifetime at the mean force turns to be quite good. It is said that $\tau(F)$ from this relation can be derived from the highly non-Gaussian rupture-force distribution, with a numerical coefficient differing by <10% [4][23].

Another preferred simple approach for data set with substantial outliers is given by [23]

$$\tau(\langle F\rangle) \approx \frac{3}{4}\delta F / \dot{F}(\langle F\rangle) \tag{2.34}$$

where $\langle F\rangle$ is the mean force, and $\delta F = F_3 - F_1$ is the interquartile range, i.e., 25% of the rupture forces are higher than F_3 and 25% are lower than F_1.

The disadvantage of using these two approximations is that experiments on different pulling speeds are necessary to get a good fit between rupture forces and lifetimes, since only one pair of $(\langle F\rangle, \tau(\langle F\rangle))$ can be extracted from one constant-speed experiment.

After getting data set $(F, \tau(F))$, use least-squares fitting logarithm of $\tau(F)$ in Eq. (2.25) with several values of ν to estimate τ_0, $\Delta x^\ddagger$, and ΔG:

$$\ln(\tau) = \ln(\tau_0) + (1 - 1/\nu)(1 - \frac{\nu F \Delta x^\ddagger}{\Delta G}) - \beta \Delta G[1 - (1 - \frac{\nu F \Delta x^\ddagger}{\Delta G})^{1/\nu}] \tag{2.35}$$

We can see that this equation is valid only when the rupture force F is below a critical force $F_c = \Delta G/(\nu \Delta x^\ddagger)$, where the barrier vanishes, or Eq. (2.35) would involve complex values due to logarithm function. If the fitting values of the tree parameters are insensitive to ν over a ν range which still lead to good fits, they are considered to be meaningful due to the independence

of the exact profile of the free-energy surface.

To validate the fitting results, we can compare the predicted force distribution according to Eq. (2.1.3) with the experimental rupture force distribution. For constant pulling speed experiments, Eq. (2.1.3) can be converted to

$$p(F|v) = \frac{1}{\dot{F}(F)\tau(F)} \frac{\exp\left[\beta(\dot{F}(F)\tau_0\Delta x^{\ddagger})^{-1}\right]}{\exp\left[\beta(\dot{F}(F)\tau(F)\Delta x^{\ddagger})^{-1}(1-\frac{\nu F\Delta x^{\ddagger}}{\Delta G})^{1-1/\nu}\right]} \tag{2.36}$$

For small loading rate $\dot{F}$, the mean rupture force $\langle F\rangle$ and the variance σ_F^2 are given asymptotically by [19][4]

$$\langle F\rangle \cong \frac{\Delta G}{\nu\Delta x^{\ddagger}}\left[1-\left(\frac{1}{\Delta G}\ln\frac{\exp(\Delta G+\gamma)}{\dot{F}\tau_0\Delta x^{\ddagger}}\right)^{\nu}\right] \tag{2.37}$$

$$\sigma_F^2 \cong \frac{\pi^2}{6\Delta x^{\ddagger 2}}\left(\frac{1}{\Delta G}\ln\frac{\exp(\Delta G+\widetilde{\gamma})}{\dot{F}\tau_0\Delta x^{\ddagger}}\right)^{2\nu-2} \tag{2.38}$$

where $\gamma = 0.5772...$ is the Euler-Mascheroni constant, $\psi''(1) = -2.404...$ is a particular value of the tetragamma function, and $\widetilde{\gamma} = \gamma^2 - 3/\pi^2\psi''(1) \approx 1.064$.[4][25] For $\nu = 1$, the phenomenological theory, the variance σ_F^2 is independent of pulling speed v. Therefore, the phenomenological approach is invalid if the experimental variance changes for different pulling speeds v.

2.1.4 Worm-like chain (WLC) model

The worm-like chain model (Kratky-Porod model) is used to describe very stiff polymers. It assumes polymers to be idealized, macroscopic, circularly-symmetric beam element with a flexural rigidity. With successive monomers constrained to point in nearly the same direction, the isotropic polymer chain is continuously flexible, different from the freely-jointed chain model, which assumes it to be flexible only between discrete segments.[26][27] The WLC model has been widely used in analyzing biological polymers, like DNA, RNA and proteins, and has some variations.[28][29][30] The basic *inextensible* WLC model describing the relation between the polymer's extension and the pulling force is summarized by the following interpolation formula

(Eq. (2.28)) [31]

$$\frac{F(x) \cdot L_p}{k_B T} = \frac{1}{4}\left(1 - \frac{x}{L_c}\right)^{-2} - \frac{1}{4} + \frac{x}{L_c}$$

where $F(x)$ is the applied force on the polymer, x is the end-to-end distance, L_c is the contour length, L_p is the persistence length of the polymer, k_B is Boltzmann constant, and T is the absolute temperature. In this formula, the polymer is treated as inextensible and persistence length L_p defines the rigidity of the chain, while the twisting effect is ignored.

While for most polymers, the elastic response cannot be neglected under stretching, two *extensible* worm-like chain (eWLC) models were derived based on the external force. For low forces ($F <\sim 10$ pN, but has limitations near $F \approx 0.1$ pN), the following interpolations formula [32]

$$\frac{F \cdot L_p}{k_B T} = \frac{1}{4}\left(1 - \frac{x}{L_c} + \frac{F}{S}\right)^{-2} - \frac{1}{4} + \frac{x}{L_c} - \frac{F}{S} \tag{2.39}$$

where parameters $F,\ x,\ L_c,\ L_p,\ k_B$ and T are same as these in Eq. (2.28), while the new parameter S, namely the elastic stretch modulus, accounts for the enthalpic term. For high forces, use the approximation [28]

$$x = L_c\left[1 - \frac{1}{2}\left(\frac{k_B T}{F L_p}\right)^{1/2} + \frac{F}{S}\right] \tag{2.40}$$

where all the parameters are same as these in Eq. (2.39).

To take into account sequence composition and a force-dependent twist-stretch coupling, a new *twistable* worm-like chain (tWLC) model was built by expanding eWLC model [30]

$$x = L_c\left[1 - \frac{1}{2}\left(\frac{k_B T}{F L_p}\right)^{1/2} + \frac{C}{-g(F)^2 + SC} \cdot F\right] \tag{2.41}$$

where $F,\ x,\ L_c,\ L_p,\ k_B,\ T$ and S are same as these in Eq. (2.39), C represents the twist rigidity, and $g(F)$ is the twist-stretch coupling [33][34][35].

2.2 Experimental materials and methods

2.2.1 Protein engineering and expression

The plasmid containing the gene encoding 8 repeats of GB1 protein with two Cysteine residues at the C-terminus (named $(GB1)_8$) was generously provided by Dr. Hongbin Li. The $(GB1)_8$ polyprotein was overexpressed in E. Coli (DH5α), and purified by Ni^{2+}-affinity chromatography (see Figure 2.3). The $(GB1)_8$ used for folding-unfolding experiments had a concentration of $\sim$ 170 µg/ml, and was kept at 4 °C in PBS buffer.

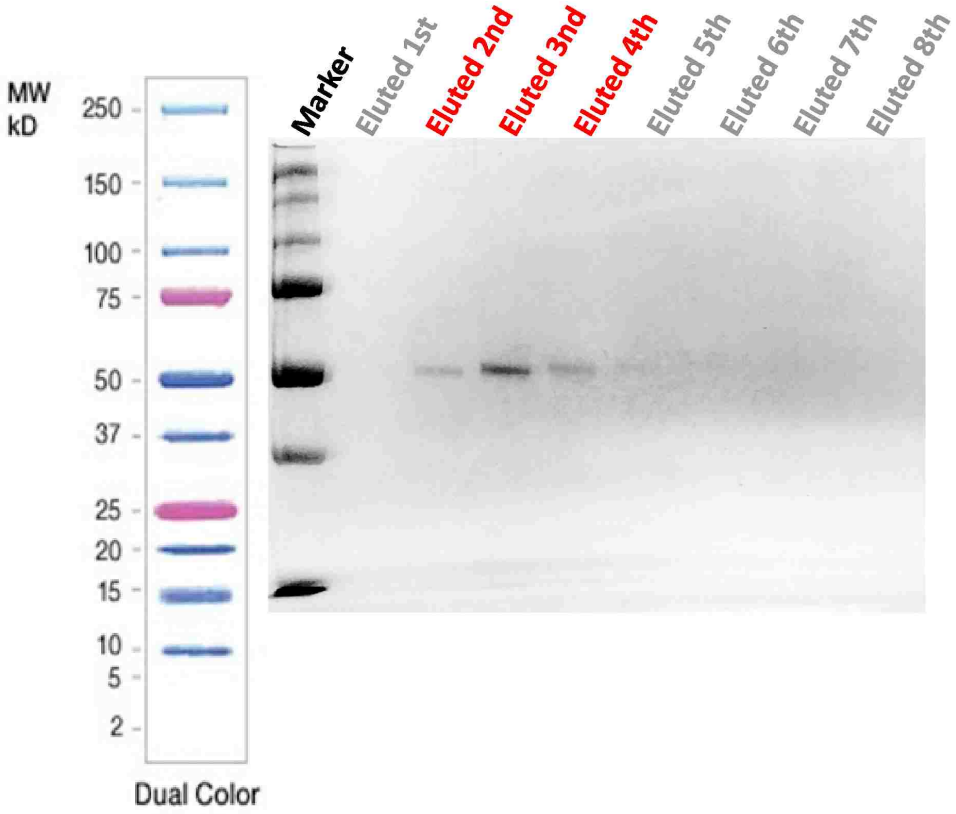

Figure 2.3: Purification of polyprotein $(GB1)_8$. SDS-PAGE gel with the molecular marker (ladder) in the left lane, as well as Dual Color Standards (from BIO-RAD) shown left. Different lanes correspond to different eluted times of supernatant with Laemmli sample buffer. GB1 has a molecular weight of $\sim$ 8 kDa, so $(GB1)_8$'s molecular weight is $\sim$ 64 kDa. The purified $(GB1)_8$, eluted twice, three and four times, appears as a predominant band on SDS-PAGE gel with an apparent molecular weight between 50 kDa and 75 kDa, in agreement with the theoretical value of $\sim$ 64 kDa.

2.2.2 Single-molecule atomic force microscopy (AFM)

The single-molecule force measurements were performed on a home-built atomic force microscopy (AFM) (see Figure 2.4) at a room temperature $\sim$ 23 °C. The AFM system uses the common beam deflection method. A beam of laser is reflected by the backside of the sensitive cantilever and detected by a position sensitive detector (PSD) with two closely spaced photodiodes. A deformation of the cantilever happens when it presses on a hard surface of the substrate. The signal's difference measured by the photodiodes is said to be proportional to the angular displacement of the cantilever. For the AFM experiments, we use a fast-speed camera (The Imaging Source DMK 21AF04.AS) to help to find the cantilever and align the laser.

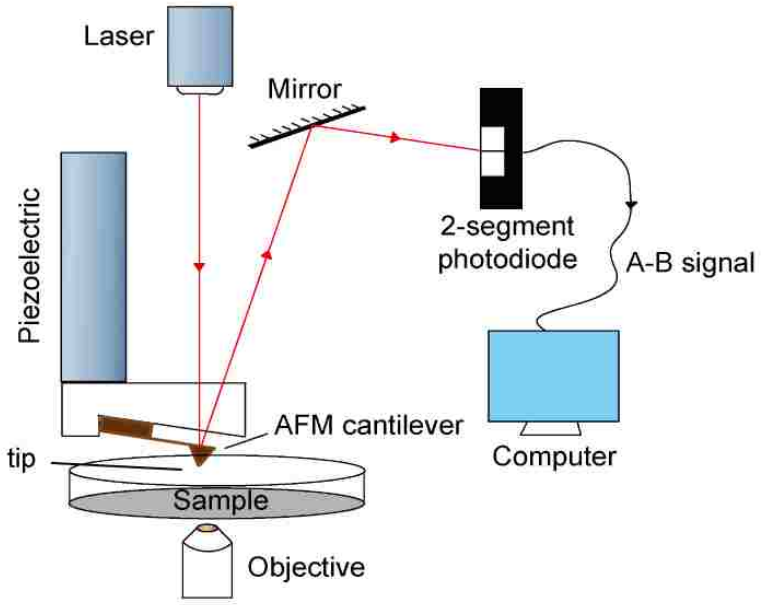

Figure 2.4: Schematic of atomic force microscopy (AFM). A beam of laser is reflected by the backside of the cantilever, and detected by a position sensitive detector (PSD) with two closely spaced photodiodes. The output signal, which is proportional the angular displacement of the cantilever, is processed in a computer.

To avoid the shifting of the gold-coated coverslip/the glass dish, some vacuum grease is placed on its bottom. The holder where the cantilever is fixed is controlled by the piezoelectric actuator. The piezoelectric actuator brings the holder down to approach and press the coverslip's surface. By setting a trigger signal, the piezo state will stop to avoid damaging the cantilever. At this time,

we can set a contact time, also called dwell time, to get a higher probability for the cantilever tip to bind to the sample (usually 1s to 5s). Which part of the polyprotein is picked up by the tip is random. The setting of dwell time depends on each experiment, and too long of a dwell time will cost much more time to finish it, especially when the pulling speed is very low (~ 0.1 μm/s). Then the cantilever moves upward to retract within a distance of Z range. If the non-specific binding force between the tip and the protein is greater than the unfolding force of some domains along the protein chain, the domain(s) will be stretched and unfold, showing a force peak when unfolding.

To measure a reliable force-extension curve of protein, we need to correct both the force exerted on the protein and the extension of it. The extension we get actually is the position of the piezo stage, so it is necessary to subtract the deformation of the cantilever when force is applied. The linear relation between the force F and the extension Δx is given by Hooke's Law: $F = -K \cdot \Delta x$ indicates that the force will also be corrected with the extension, where K is the spring constant of cantilever.

Besides, since all the AFM experiments are carried in a liquid environment, we need to consider the hydrodynamic effects, especially when the solvent viscosity is strong and the pulling speed is high. To quantify the hydrodynamic effects, we measure the force extension curve inside the solution, but without touching the substrate's surface.

2.2.3 Single molecule experiments

For our experiments, all the force-extension measurements were done in liquid solution at room temperature. The basic solution is filtered phosphate-buffered saline (PBS) (1X, pH 7.4). In order to investigate the effects of denaturation and the solvent viscosity on the protein unfolding mechanisms, we did the single-molecule experiments using a home-built AFM at six different pulling speeds for each concentration (0M, 1M, and 2M) of denaturation guanidinium chloride (GdmCl), as well as various concentrations (0%, 10%, 20%, and 30%) of glycerol to change the solvent viscosity.

In a typical experiment, ~ 10 μL of $(GB1)_8$ protein solution was deposited onto a clean gold-coated coverslip covered by ~ 150 μL specified solution mentioned above. To make sure that $(GB1)_8$ is well bound to the gold-coated surface, we usually waited for ~ 15 minutes before pulling experiments proceeded, and also the solution would be more stabilized.

Since we don't want to calibrate the cantilever when it is contaminated after experiments, we measure the thermal oscillation with the cantilever suspended in PBS solution, and the relation between the angular displacement (piezo's extension) with the detected output signal on a hard glass dish before pulling the polyprotein $(GB1)_8$. The cantilever we usually used is the largest Silicon Nitride cantilever ("C" cantilever) of Bruker AFM Probes (model: MLCT), with a normal spring constant of 0.01 N/m (varying from 0.005 N/m to 0.02 N/m). The spring constant is usually calculated by using thermal vibrations [36]

$$\frac{1}{2}K\langle x^2\rangle = \frac{1}{2}k_BT \tag{2.42}$$

where K and $\langle x^2\rangle$ denote the spring constant and the time-average square of the thermal fluctuation of the cantilever, respectively; k_B is Boltzmann constant, and T is absolute temperature of the cantilever. The time-average "thermal energy" ($\frac{1}{2}K\langle x^2\rangle$) is calculated in the frequency domain according to Parseval's theorem

$$\int |x(t)|^2 \mathrm{d}t = \int |x(\omega)|^2 \mathrm{d}\omega \tag{2.43}$$

Through this thermal fluctuation method, the error of the spring constant calibrated varies between 10% - 20%.

2.3 Internal friction

The effects of solvent viscosity on protein folding/unfolding dynamics have been studied through both experimental methods and simulation.[37][9][6] It is shown that protecting osmolytes, such

as glycerol and sarcosine, can slow down the intrinsic unfolding rate of a globular protein while accelerate its folding rate concurrently, independent of the applied force and without any complexion at the transition state. The result agrees with Kramers theory [1] of Eq. (2.2) at a strong viscosity limit, due to the friction factor γ in the expression. However, since Kramers derived the expression by simplifying the reaction process to a simple one-dimensional diffusion process, the rate of escape k deduced actually represents the overall rate, with an "effective" friction coefficient γ accounting for all the mechanisms that the energy can dissipate out during the reaction process. The friction coefficient γ, at least, includes the effects of both solvent dynamic friction η and the internal friction σ. In 2012, Andrea Sorannoa *et al.* [10] quantified the contribution of solvent-independent internal friction in unfolded and intrinsically disordered proteins with single-molecule spectroscopy, by a variation of solvent viscosity η and extrapolation to $\eta = 0$ [38].

Ansari *et al.* [8] found that the rate k of conformational relaxation in myoglobin can be described by

$$k = \frac{C}{\sigma + \eta} \exp(-E_0/k_B T) \tag{2.44}$$

where $C,\ \sigma,\ E_0$ are constant, and σ has units of viscosity and can be regarded as internal friction. And earlier Beece *et al.* [7] reported a power-law behavior in the viscosity-dependence of ligand binding in myoglobin. Based on these results, we develop a new expression to firstly quantify the external friction on GB1 unfolding experiments, i.e.,

$$\tau_0 = k_0^{-1} = C(\sigma + \eta)^d \tag{2.45}$$

where τ_0 and k_0 denote the intrinsic lifetime and the spontaneous unfolding rate, respectively; C and d are the adjustable parameters; σ and η represent the solvent friction and internal friction, respectively.

For our experiments, after extracting the kinetic parameters of k_0 or τ_0 in different solvent viscosities, we can fit the solvent-viscosity-depend spontaneous unfolding rate to Eq. (2.45),

which leads to a quantified internal friction during the protein unfolding/folding process.

Chapter 3

Experimental Results

3.1 Structure of the artificial elastomeric polyprotein $(GB1)_8$

GB1 protein is a classical paradigm for studying the protein folding/unfolding process in single molecular experiments. It is a small, very regular α/β structure composed of 56 animo acids (approximately 8kDa molecular weight). The fold consists of a four-stranded β-sheet and a long α-helix tightly packed against the sheet (Figure 3.1).[39][40] The β-sheet has two symmetrically spaced hairpins: one is formed by N-terminal strands and the first β turn (β1-turn1-β2), and the other formed by C-terminal strands and the second β turn (β3-turn2-β4). The mechanical folding/unfolding dynamics of the monomer protein GB1 has already been well studied through both thermal and chemical denaturation approaches.[41][42][43][44][45] **The first goal of our study** is to investigate the mechanical stability and energy landscape of GB1 protein, and identify the contribution of solvent viscosity and denaturant. To realize this goal, we constructed a polyprotein of $(GB1)_8$ which is a tandem repeat of eight identical units of GB1 (Figure 3.1), and pulled the polyprotein at different concentrations of glycerol, and different concentrations of denaturant GdmCl. Experiments were conducted at different constant pulling speeds.

When stretching the polyprotein $(GB1)_8$ with AFM, the eight domains unfold one by one under external force, but unnecessarily from the first one at one end to the last at the other end.

As a consequence, it gives a characteristic saw-tooth pattern of the force-extension curves shown in Figure 3.1 from our experimental results. The characteristic saw-tooth pattern has several equally spaced force peaks, depending on how many **folded** GB1 domains are stretched during the single approach and retract process. If all the eight GB1 domains of polyprotein $(GB1)_8$ are pulled and unfolded, there are usually up to ten force peaks, eight of which are the unfolding force peaks. The first peak (at the left beginning, shown in Figure 3.1) of the curve corresponds to the non-specific adhesion between the protein and the gold-coated surface, while the last peak corresponds to the detachment of the protein from the AFM tip or substrate, and usually it should be from the AFM tip since the GB1 protein is covalently bound to gold-coated surface through thiols (-SH).

For our experiments, we did the single-molecule experiments using a home-built AFM at six different pulling speeds for each concentration (0M, 1M, and 2M) of denaturation guanidinium chloride (GdmCl), as well as various concentrations (0%, 10%, 20%, and 30%) of glycerol to change the solvent viscosity. Figure 3.1 shows a typical force-extension curve obtained from our $(GB1)_8$ pulling experiments. The dark lines were plotted with the experimental data collected, showing a characteristic saw-tooth pattern. The colored lines were plotted by least squares fit to worm-like chain (WLC) model.

The relation between the proteins' extension and the pulling force can be characterized by the inextensible WLC model with Eq. (2.28)

$$\frac{F \cdot L_p}{k_B T} = \frac{1}{4}\left(1 - \frac{x}{L_c}\right)^{-2} - \frac{1}{4} + \frac{x}{L_c}$$

where F is the applied force on the protein, x is the end-to-end distance, L_c is the contour length, L_p is the persistence length, k_B is Boltzmann constant, and T is the absolute temperature. By fitting consecutive force peaks, we calculated the contour length increment ΔL_c, namely the elongation of GB1 monomer during mechanical unfolding process. Meanwhile, we also acquired some information about the elasticity of the polyprotein $(GB1)_8$ from the fitted parameter L_p.

3.1.1 Results

The contour length increment ΔL_c of GB1

Applying WLC model to fit each unfolding force peak of good force-extension curves, we found that the pulling speeds, varying from 0.1 μm/s to 5 μm/s, had little effect on the contour length

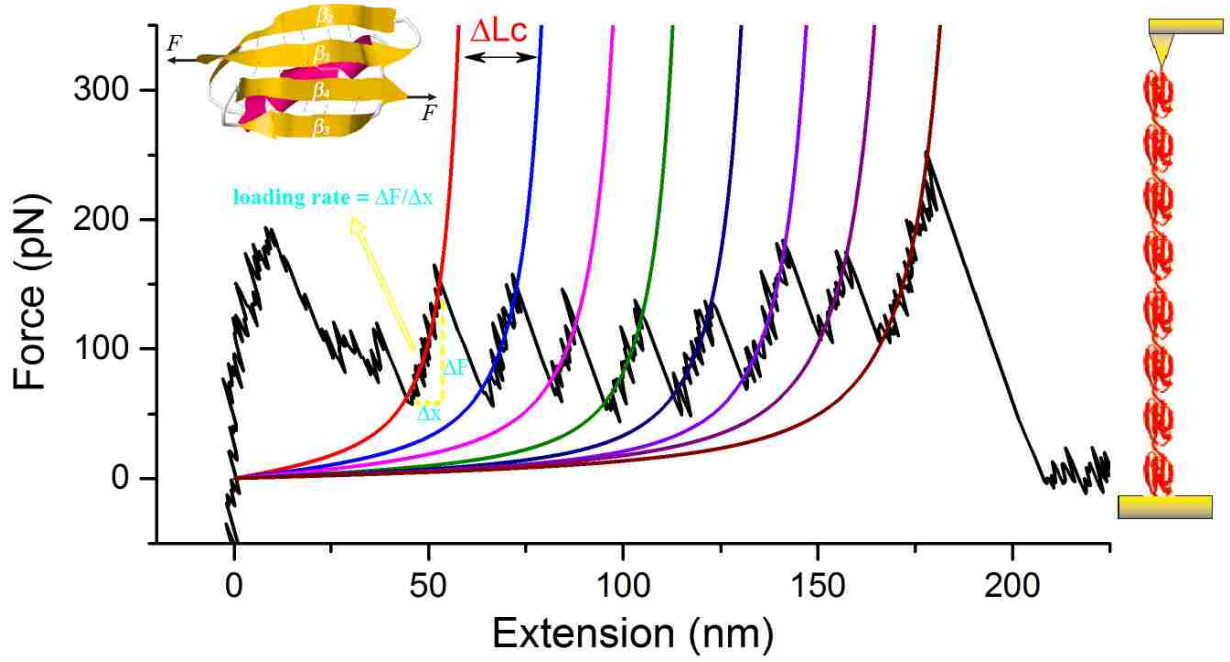

Figure 3.1: Typical force-extension curve of polyprotein $(GB1)_8$. The force-extension curve was obtained for PBS buffer at 1M GdmCl, 20% (v/v) Glycerol. The stretching force-extension curve (black line) shows a characteristic saw-tooth pattern, with equally spaced force peaks, due to the consecutively mechanical unfolding of each GB1 domain in the polymer chain. The beginning part of the curve corresponds to the non-specific adhesion between the protein and the gold-coated surface, while the last peak to the the detachment of the protein from the AFM tip or substrate. Seven individual unfolding force peaks can be definitely classified from the force-extension curve, and it can have up to eight unfolding force peaks. ΔL_c is the increment of contour length for consecutive unfolding force peaks fitted by WLC model (colored lines), corresponding to the length difference between the unfolded state and folded state of GB1 monomer. As shown, we use formula $\dot{F} = \Delta F/\Delta x$ to calculate the force loading rate, where ΔF and Δx denote the unfolding force and the extension of an individual GB1 domain, respectively. A cartoon drawing of GB1's three-dimensional structure (PDB code 1pgb) is on the top left corner and a cartoon schematic diagram of $(GB1)_8$ was adopted from [11]. GB1 is an α/β-protein with the two terminal β-strands (strands 1 and 4) arranged in parallel; they are bonded by a series of backbone hydrogen bonds (indicated by dashed purple lines), which can form mechanical resistance to unfolding when stretched. For the construction of $(GB1)_8$, eight identical GB1 monomers are combined in tandem by connecting the N- and C-terminal.

increment ΔL_c and the persistence length L_p, since that the conformation of polyprotein $(GB1)_8$ was not easily changed by pulling speeds. Therefore, we ignored the difference of pulling speeds, and turned to analyze the contribution of different concentrations of GdmCl and glycerol to ΔL_c and L_p.

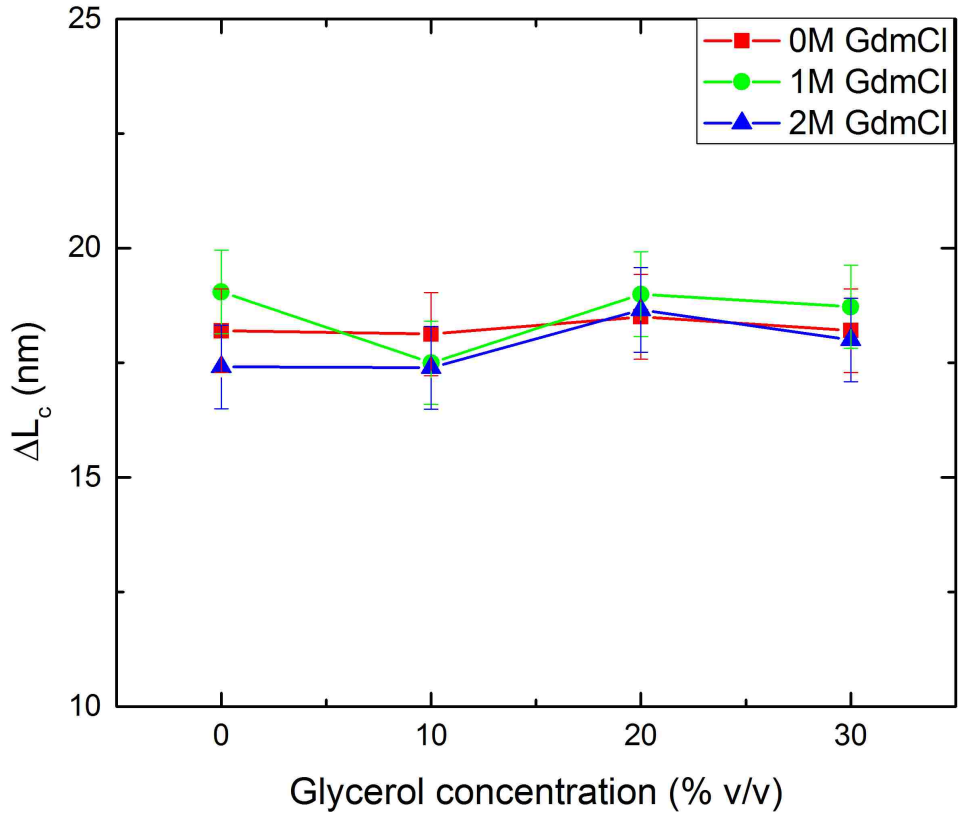

Figure 3.2: Contour length increment between consecutive force peaks. The contour length increment ΔL_c of GB1 is plotted versus the glycerol concentration. The filled symbols represent the *most probable* contour length increment for different pulling speeds in each particular solution, by fitting to WLC model with Eq. (2.28). The presence of denaturant GdmCl and glycerol has little effect on ΔL_c. The fitted ΔL_c is $\sim$ 18 nm, in good agreement with previous results [11].

Figure 3.2 shows the fitted results of contour length increment ΔL_c for different concentrations of GdmCl and glycerol. Each contour length increment ΔL_c shown here is the *most probable* contour length increment for different pulling speeds in each particular solution. For pure PBS (0M GdmCl, 0% glycerol), the contour length increment $\Delta L_c = 18.1 \pm 0.9$ nm ($n = 57$); for PBS (2M GdmCl, 0% glycerol), the contour length increment $\Delta L_c = 17.4 \pm 0.9$ nm ($n = 61$).

It indicated that the GB1 domain elongated by roughly ~ 18 nm on its mechanical unfolding. Similar results were obtained for different concentrations of glycerol. A regular GB1 domain has 56 animo acids, thus is ~ 20.2 nm (56 aa $\times$ 0.36 nm/aa) long when it is fully stretched. Since the length of the folded GB1 domain (the distance between its N- and C- termini) is 2.6 nm [39], the mechanical unfolding of a GB1 domain makes it to extend by 17.6 nm. Our fitted contour length increment between consecutive peaks according to WLC model agrees with this value quite well. Moreover, within allowable error, the contour length increment ΔL_c is not affected by the chemical denaturant and solvent viscosity.

The persistence length L_p of GB1

The persistence length is used to quantify the stiffness of a polymer, and has been widely used in single molecular experiments. By fitting to WLC model with Eq. (2.28), we found out how the denaturant and glycerol influenced the stiffness of the GB1 protein.

Figure 3.3 shows the fitted persistence length of GB1 versus the glycerol concentration in different concentrations of GdmCl (0M, 1M, and 2M). For PBS (0M GdmCl, 0% glycerol), the persistence length $L_p = 0.55 \pm 0.34$ nm ($n = 70$); for PBS (0M GdmCl, 30% glycerol), the persistence length $L_p = 0.47 \pm 0.21$ nm ($n = 72$). For all the conditions, the minimum value of the persistence length is roughly ~ 0.22 nm, while the maximum value of that is roughly ~ 0.57 nm. All the values of L_p are approximately 1 nm, so we concluded that the GB1 domain keeps the same stiffness and elasticity with the presence of denaturant GdmCl and different concentrations of glycerol.

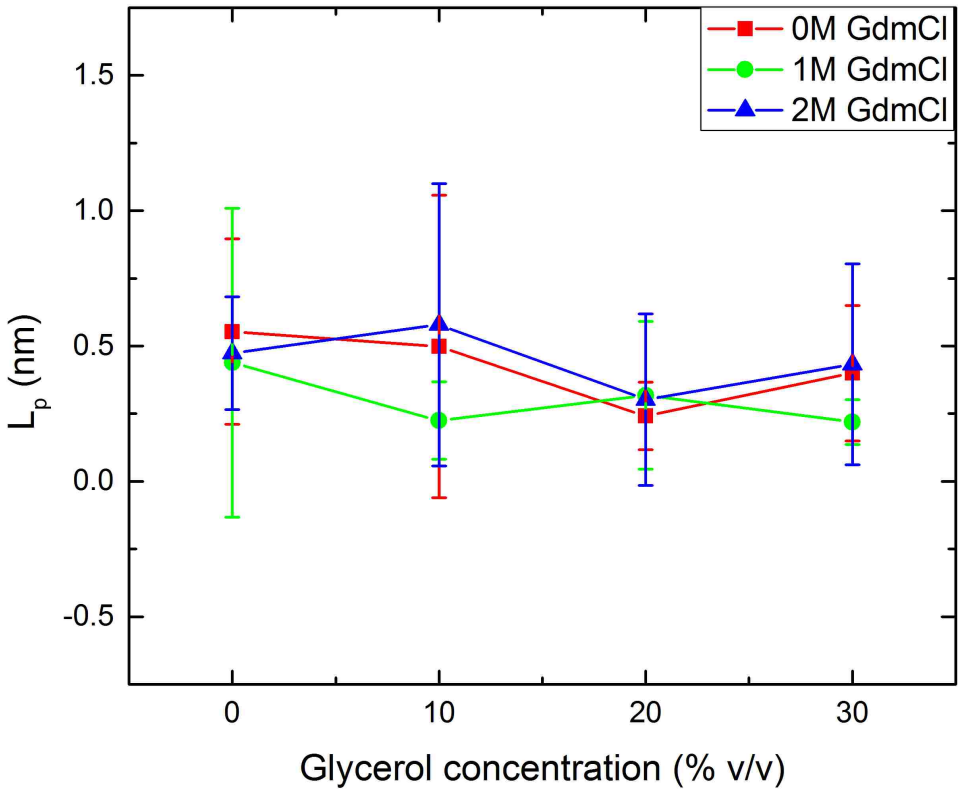

Figure 3.3: Persistence length of GB1 protein. The persistence length of GB1 is plotted versus the glycerol concentration. The filled symbols represent the *average* persistence length for different pulling speeds in each particular solution, by fitting to WLC model with Eq. (2.28). The presence of denaturant GdmCl and different solvent viscosities have little effect on L_p, since the values of L_p are approximately 1 nm.

3.2 Bell-Evans model

In Chapter 3.1, we have already known the effects of chemical denaturant GdmCl and the solvent viscosity on the structure and elasticity of protein GB1 quantitatively. In this section and next section, we used two most popular models to extract the kinetic properties of protein GB1, and studied how the chemical denaturant GdmCl and solvent viscosity change the protein's stability and energy landscape.

According to Bell-Evans model (Chapter 2.1.2), with the unfolding force histograms at different pulling speeds, we were able to extract the spontaneous unfolding rate k_0 and the location of the transition state $\Delta x^{\ddagger}$ by fitting the relation between the most probable force F^* and the force loading rate $\dot{F}$ to Eq. (2.14):

$$F^*(\dot{F}) = \frac{1}{\beta \Delta x^{\ddagger}} \ln(\frac{\beta \Delta x^{\ddagger}}{k_0} \dot{F}) = \frac{1}{\beta \Delta x^{\ddagger}} \ln(\dot{F}) + \frac{1}{\beta \Delta x^{\ddagger}} \ln(\frac{\beta \Delta x^{\ddagger}}{k_0})$$

where $\beta = (k_B T)^{-1}$ is the thermal factor. Note that Evans *et al.* [3] used a force scale, f_β, to represent $\beta \cdot \Delta x^{\ddagger}$ in their papers.

The unfolding force distributions of GB1 protein at different solvent conditions are shown in Figure 3.7, with a constant pulling speed $v = 0.52$ μm/s. We set the bin width $\Delta F = 25$ pN. For our experiments, we pulled the polyprotein $(GB1)_8$ at three concentrations of GdmCl (0M, 1M, and 2M) and four different glycerol concentrations (0%, 10%, 20%, and 30%), with six different pulling speeds v (∼0.1μm/s, ∼0.2μm/s, ∼0.5μm/s, ∼1μm/s, ∼2μm/s, ∼5μm/s). The most probable unfolding force for each condition was calculated by fitting the histogram to a Gaussian distribution (not shown), while the loading rate was calculated with the simple expression $\dot{F} = Kv$ (shown in Figure 3.1), where K is the cantilever's spring constant, and v is the pulling speed. Before fitting the datasets of (F^*, $\dot{F}$) pairs, we took a look at the force histograms. It has been demonstrated that the analysis of force distribution provides information about the underlying free-energy landscape [46][47][48], and the width of the force histogram is directly related to the distance $\Delta x^{\ddagger}$ between the folded state and the transition state along the mechanical un-

folding reaction coordinate [3]. As shown in Figure 3.7, the width of unfolding force histograms at different conditions remained nearly unchanged (comparable with previous results $\sim$ 55 pN [12]), indicating that the distance between the folded state and the transition state was unaltered by chemical denaturants. To further verify this conclusion, we turned to analyze the relation between the most probable force and the loading rate.

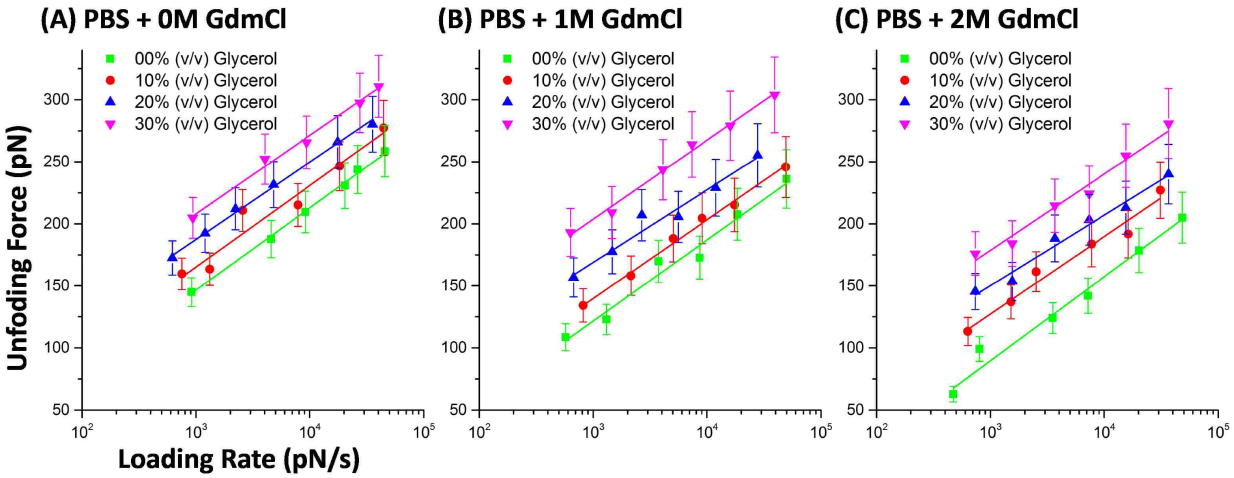

Figure 3.4: The most probable unfolding force as a function of loading rate for various glycerol concentrations and different GdmCl concentrations: **(A)** 0M GdmCl, **(B)** 1M GdmCl, and **(C)** 2M GdmCl. The most probable force F^* is plotted versus the force loading rate $\dot{F}$. The filled symbols represent the data of most probable force calculated by Gaussian fit to the unfolding force histograms, and the loading rate calculated by $\dot{F} = K \cdot v$, where K is the spring constant of cantilever, and v is the pulling speed. Colored solid lines represent linear least squares fits to Bell-Evans model.[2][3][49] The fitting parameters are shown in Table 3.1.

3.2.1 Results

According to the fitting results, for pure PBS solution (0M GdmCl, 0% glycerol), the spontaneous unfolding rate constant of GB1 domain is $k_0 = 0.213 \pm 0.020$ s^{-1}, corresponding to an intrinsic lifetime of $\tau_0 = k_0^{-1} \approx 4.69$ s, and the distance between the unfolded state and the transition state $\Delta x^{\ddagger} = 1.62 \pm 0.15$ Å.

η	0M GdmCl		1M GdmCl		2M GdmCl	
(mPa s)	k_0 (s^{-1})	$\Delta x^{\ddagger}$ (Å)	k_0 (s^{-1})	$\Delta x^{\ddagger}$ (Å)	k_0 (s^{-1})	$\Delta x^{\ddagger}$ (Å)
0.86	0.213 ± 0.020	1.62 ± 0.15	0.486 ± 0.025	1.59 ± 0.11	1.609 ± 0.110	1.64 ± 0.10
1.20	0.114 ± 0.011	1.68 ± 0.20	0.228 ± 0.015	1.61 ± 0.21	0.538 ± 0.021	1.65 ± 0.13
1.70	0.036 ± 0.002	1.65 ± 0.20	0.051 ± 0.003	1.63 ± 0.12	0.092 ± 0.003	1.73 ± 0.22
2.57	0.018 ± 0.002	1.70 ± 0.16	0.022 ± 0.001	1.68 ± 0.12	0.032 ± 0.002	1.69 ± 0.21

Table 3.1: Extracted mechanical properties for unfolding of protein GB1 obtained by least squares fit to Bell-Evans model with Eq. (2.14). The datasets used to fit include the most probable force calculated by Gaussian fit to the unfolding force distribution at different concentrations of denaturant GdmCl (0M, 1M, and 2M) and various concentrations of glycerol (0%, 10%, 20%, and 30%), and the corresponding force loading rate $\dot{F}$, calculated simply by $\dot{F} = Kv$, where K is the spring constant of cantilever, and v is the constant pulling speed.

Chemical denaturants speed up the mechanical unfolding process

As shown before, the mechanical unfolding pathway is not changed by the chemical denaturant due to the little change of the contour length increment ΔL_c. By comparing the spontaneous unfolding rate in the presence of chemical denaturation and glycerol, we can quantitatively tell their effects according to Table 3.1.

Figure 3.5 shows the plot of spontaneous unfolding rate versus the solvent viscosity at different concentrations of GdmCl. As the concentration of chemical denaturant increased, the spontaneous unfolding rate k_0 increased from 0.213 s^{-1} to 1.609 s^{-1} for solution without any glycerol; k_0 increased from 0.114 s^{-1} to 0.538 s^{-1} for solution with 10% glycerol; k_0 increased from 0.036 s^{-1} to 0.092 s^{-1} for solution with 20% glycerol; k_0 increased from 0.018 s^{-1} to 0.032 s^{-1} for solution with 30% glycerol. Therefore, the chemical denaturants speed up the spontaneous unfolding rate of protein GB1 by $2 \sim 7$ times, and the mechanical stability of protein GB1 is decreased.

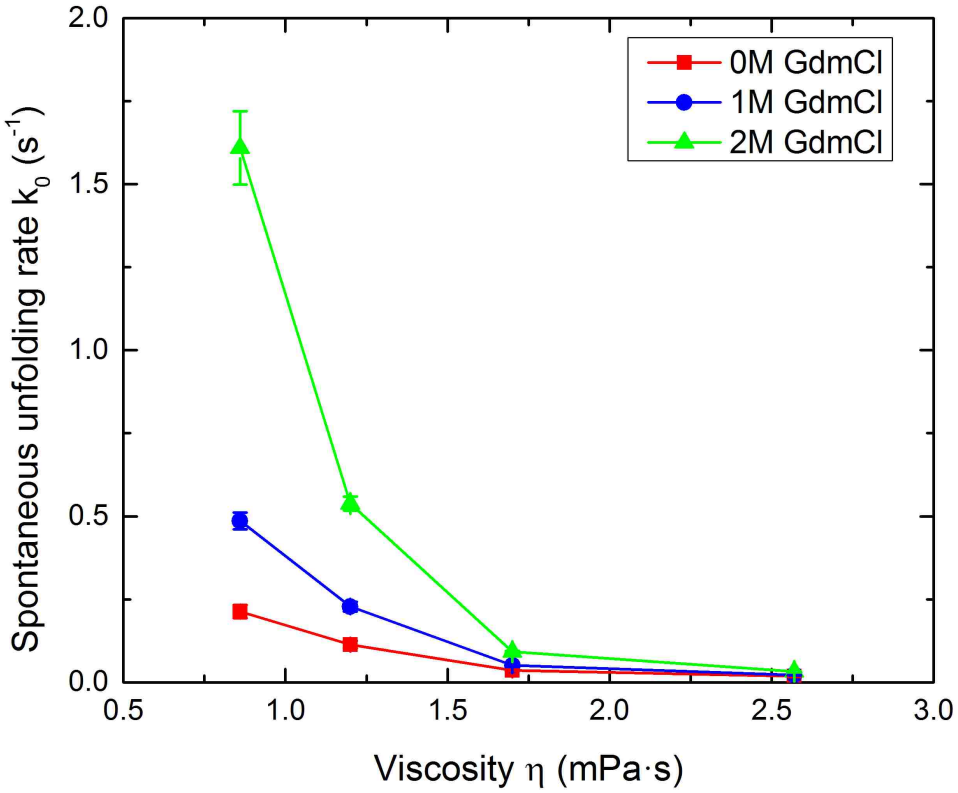

Figure 3.5: Spontaneous unfolding rate as a function of solvent viscosity at different denaturant concentrations. The spontaneous unfolding rate k_0 of GB1 is plotted versus the solvent viscosity η. The filled symbols represent the data from Table 3.1. The spontaneous unfolding rate of GB1 increased with the increase of GdmCl concentration, from ~ 0.213 s^{-1} in PBS (0M GdmCl, 0% glycerol) to ~ 1.609 s^{-1} in PBS (2M GdmCl, 0% glycerol), while decreased to ~ 0.018 s^{-1} as the glycerol concentration increases to 30%, without GdmCl.

Glycerol slows down the mechanical unfolding process

The experimental results also provided enough information about the function of glycerol or solvent viscosity in the mechanical unfolding process of GB1. According to Table 3.1 (shown in Figure 3.5), as the solvent viscosity increased from 0.86 mPa s to 2.57 mPa s (corresponding to 0% glycerol$\rightarrow$30% glycerol), the spontaneous unfolding rate k_0 decreased from 0.213 s^{-1} to 0.018 s^{-1} for solution without any chemical denaturant; k_0 decreased from 0.486 s^{-1} to 0.022 s^{-1} for solution at 1M GdmCl; k_0 decreased from 1.609 s^{-1} to 0.032 s^{-1} for solution at 2M GdmCl. It is evident that the increase of solvent viscosity greatly slows down the mechanical unfolding process, while no active complexation of the glycerol molecules involves into the unfolding

transition state.

The mechanical unfolding distance is unaltered by denaturant

From the fitted parameter $\Delta x^{\ddagger}$, the activation location, we can tell how the shape of the energy landscape of GB1 unfolding process changes.

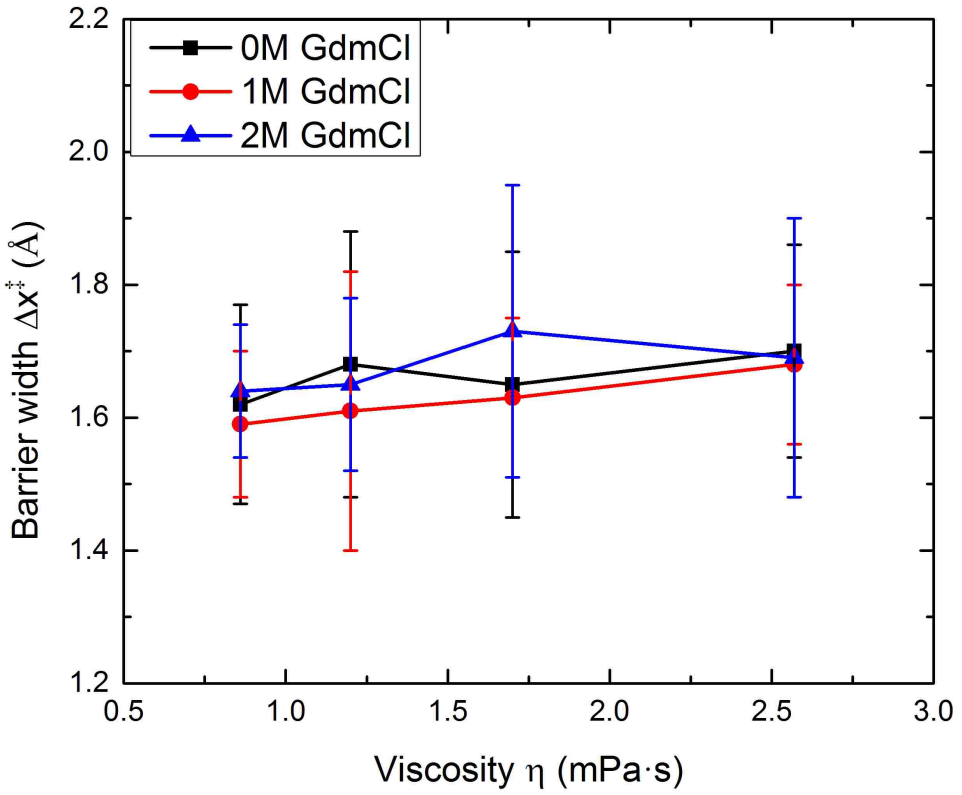

Figure 3.6: The distance between the folded state and the transition state. The unfolding distance $\Delta x^{\ddagger}$ of GB1 is plotted versus the solvent viscosity η. The filled symbols represent the data from Table 3.1. The value of $\Delta x^{\ddagger}$ is ~ 1.7 Å with a small fluctuation for different concentrations (0M, 1M, and 2M) of denaturant GdmCl in various viscosities of solution (0% glycerol, 10% glycerol, 20% glycerol, and 30% glycerol).

Figure 3.6 shows the plot of the fitted distance $\Delta x^{\ddagger}$ between the native folded state and the transition state for different concentrations of GdmCl, according to Table 3.1. We can see that the value of $\Delta x^{\ddagger}$ is $\sim$ 0.17 Å. In the absence of chemical denaturant GdmCl, we obtained 1.62 ± 0.15 Å $\leq \Delta x^{\ddagger} \leq 1.70 \pm 0.16$ Å for various solvent viscosities ranging from ~ 0.86 mPa s to ~ 2.57 mPa s; for solution with 1M GdmCl, we obtained 1.59 ± 0.11 Å $\leq \Delta x^{\ddagger} \leq 1.68 \pm 0.12$ Å;

and for solution with 2M GdmCl, we obtained 1.64 ± 0.10 Å $\leq \Delta x^{\ddagger} \leq 1.73 \pm 0.22$ Å. It is reported that $\Delta x^{\ddagger}$ is $\sim$ 1.7 Å to $\sim$ 2.0 Å [12][50], matching with our results well. Our data suggested that the mechanical unfolding distance $\Delta x^{\ddagger}$ was unaltered by the denaturant.

Although the height of the activation energy was not directly given by the model, the fact that the chemical denaturant increased the spontaneous unfolding rate constant predicted that the height of barrier was reduced by the denaturant, and the increase of solvent viscosity decreased the spontaneous unfolding rate indicated that the energy needed to activate GB1 was increased by the glycerol.

3.3 Dudko model

Dudko's model was utilized to extract kinetic information from single molecule experiments, basically by transforming the unfolding force histograms obtained at different loading rates into the force-dependent lifetimes which are measurable in constant-force experiments. The kinetic information includes (1) the intrinsic lifetime τ_0; (2) the location of the transition state $\Delta x^{\ddagger}$; (3) the apparent free energy of activation ΔG.

For each constant-velocity pulling experiments, we first constructed smooth unfolding force histograms. Then we got the (force, lifetime) pairs by transforming the histograms according to Eq. (2.32)

$$\tau(F_i) = \frac{\left(p(F_i)/2 + \sum_{k=i+1}^{N} p(F_i)\right) \cdot \Delta F}{\dot{F}(F_i) \cdot p(F_i)}$$

where $F_i = F_{min} + (i - 1/2)\Delta F$, for $1 \leq i \leq N-1$; $\tau(F_N) = \frac{p(F_N)/2 \cdot \Delta F}{\dot{F}(F_N) \cdot p(F_N)} = \frac{\Delta F}{2\dot{F}(F_N)}$, for $i = N$. It has been predicted that all the (force, lifetime) pairs should collapse onto one single master curve, in spite of the different pulling speeds.

For data analysis, we set $\Delta F = 25$ pN. There were 6 groups of (force, lifetime) pairs due to the 6 different loading rates $\dot{F}$ or pulling speeds v ($\sim$0.1μm/s, $\sim$0.2μm/s, $\sim$0.5μm/s, $\sim$1μm/s, $\sim$2μm/s, $\sim$5μm/s). Since we didn't add any linkers to the polyprotein $(GB1)_8$ through the experiments, there was no need to apply the linker-effect correction described in Eq. (2.29). The unfolding-force histograms are shown in Figure 3.7 and Figure 3.8 is the transformation for pulling polyprotein $(GB1)_8$ in PBS buffer + 0M GdmCl + 30% Glycerol, according to Eq. (2.32). The prediction that all the (force, unfolding time) pairs for different pulling speeds collapse onto a single master curve was validated here. It is noticed that the logarithm of the extracted lifetime depended nonlinearly on the unfolding force, so it cannot be well described by the Bell-Evans model (Eq. (2.6)). We used least squares to fit the data in Figure 3.8 according to Dudko's model, with Eq. (2.25) (or Eq. (2.26))

$$\tau(F) = \tau_0(1 - \frac{\nu F \Delta x^{\ddagger}}{\Delta G})^{1-1/\nu} \cdot \exp\{-\beta \Delta G[1 - (1 - \frac{\nu F \Delta x^{\ddagger}}{\Delta G})^{1/\nu}]\}$$

For Figure 3.8, we obtained that $\tau_0 = 157.0 \pm 8.0$ s, $\Delta x^{\ddagger} = 1.88 \pm 0.24$ Å, and $\Delta G = 30.9 \pm 4.0$ k_BT for $\nu = 1/2$, whereas $\tau_0 = 121.6 \pm 8.0$ s, $\Delta x^{\ddagger} = 1.75 \pm 0.15$ Å, and $\Delta G = 26.8 \pm 3.0$ k_BT for $\nu = 2/3$. The fitted curve with $\nu = 1/2$ is shown in Figure 3.8 by the solid line, while the fit with $\nu = 2/3$ is not shown (comparable). Using the same procedure, we extracted the key mechanical landscape parameters (τ_0, $\Delta x^{\ddagger}$, and ΔG) for pulling polyprotein $(GB1)_8$ in PBS buffer with different concentrations of denaturant GdmCl and various glycerol concentrations, and summarized them in Table 3.2. Before deducing any reliable conclusions from Table 3.2, we need to firstly make sure that the key landscape parameters fitted to Dudko's model are reasonable. To validate the fitting parameters, we turned to Eq. (2.1.3) and the more explicit equation for our constant-speed experiments, Eq. (2.36)

$$p(F|v) = \frac{1}{\dot{F}(F)\tau(F)} \frac{\exp\left[\beta(\dot{F}(F)\tau_0\Delta x^{\ddagger})^{-1}\right]}{\exp\left[\beta(\dot{F}(F)\tau(F)\Delta x^{\ddagger})^{-1}(1-\frac{\nu F\Delta x^{\ddagger}}{\Delta G})^{1-1/\nu}\right]}$$

where $p(F|v)$ is the *predicted* probability density for unfolding force F at constant pulling speed v; $\dot{F}(F)$ is the force loading rate at force F, for our constant-peed experiments, $\dot{F}(F) = Kv$, where K is the spring constant for the the stiff molecular system; $\tau(F)$ is the lifetime under external force F which can be calculated with Eq. (2.25); $\beta = (k_BT)^{-1}$ is a known constant thermal factor; τ_0, $\Delta x^{\ddagger}$, and ΔG are the three key mechanical parameters, which were obtained by least squares fitting to Eq. (2.25), see Table 3.2; and ν is the scaling factor, corresponding to different kinds of free-energy surface profile. After calculating the force probability distribution function $p(F|v)$, we multiplied $p(F|v)$ with $\Delta F (= 25$ pN) and compared the probability $p(F|v)\Delta F$ with the experimental unfolding force histograms. Figure 3.7 shows both the experimental unfolding force histograms and the *predicted* unfolding force histograms. All the experimental unfolding-force histograms shown were obtained at a constant pulling speed $v = 0.52$ μm/s. The solid lines are the *predicted* unfolding force probabilities for different concentrations (0M, 1M, and 2M) of GdmCl and various concentrations (0%, 10%, 20%, and 30%) of glycerol under constant loading rates $\dot{F}(F)$ (or pulling speeds v), obtained by plotting the unfolding-force distributions with the

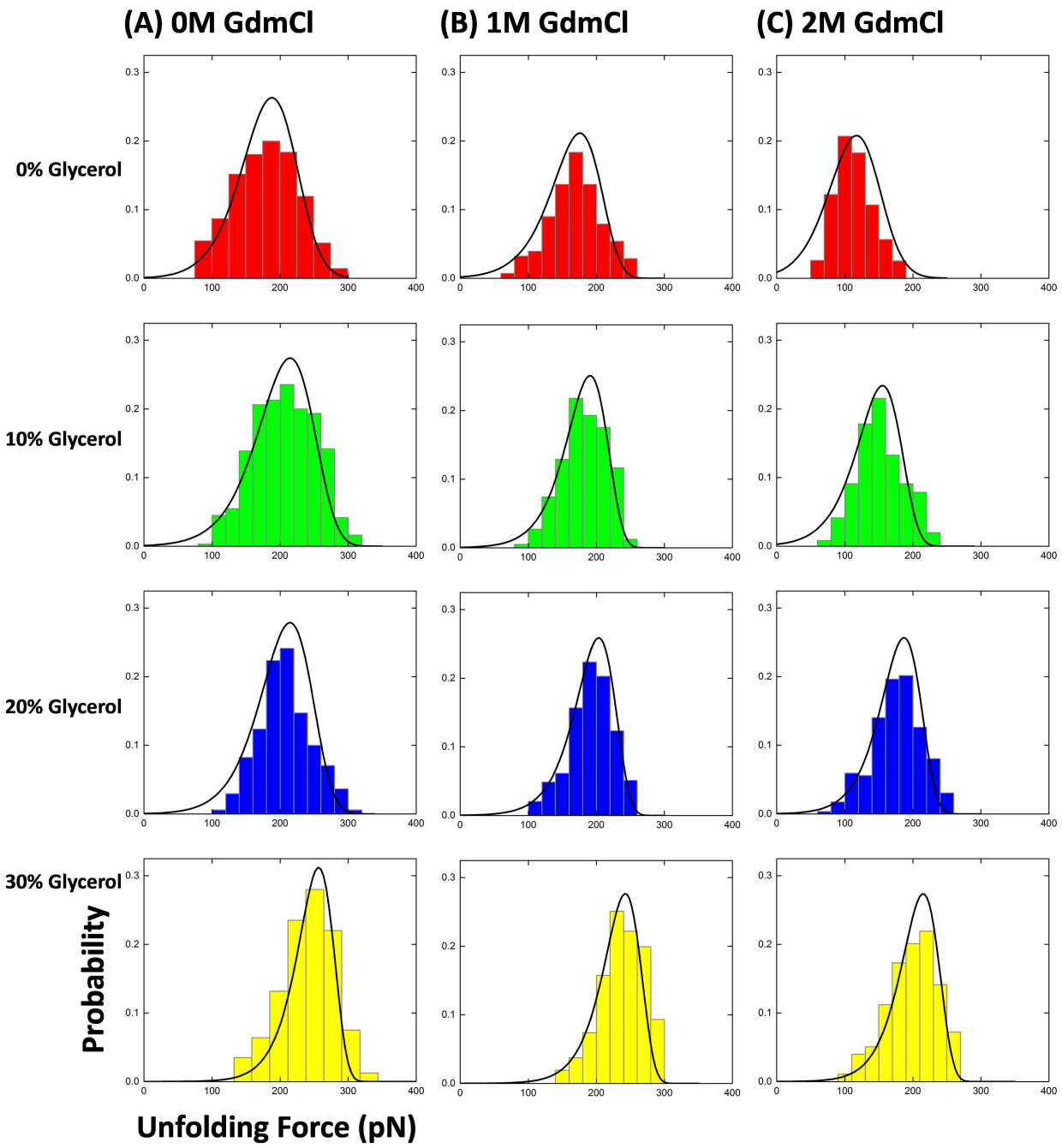

Figure 3.7: Unfolding force histograms for pulling polyprotein $(GB1)_8$ with a home-built AFM, at a constant pulling speed $v = 0.52$ μm/s. Colored histograms are obtained from experimental data for various glycerol concentrations (0%, 10%, 20%, and 30%) at different GdmCl concentrations (A. 0M, B. 1M, and C. 2M), setting $\Delta F = 25$ pN. Black solid lines are the *predicted* unfolding force distributions with the parameters (shown in Table 3.2) extracted from the least-squares fit of Eq. (2.25) (or Eq. (2.35)) to the collapsed data from Eq. (2.32), with scaling factor $\nu = 2/3$.

parameters extracted from the least-squares fit, with scaling factor $\nu = 2/3$, of Eq. (2.25) (or Eq. (2.35)) to the collapsed data from Eq. (2.32). It is clear that all the *predicted* unfolding-force distributions agreed with the experimental results quite well, meaning that the fitted parameters shown in Table 3.2 are reliable. Actually, the extracted parameters were relatively insensitive to ν and thus similar results were observed. Moreover, we realized that the real unfolding-force distributions were very close to Gaussian distribution, but not over the entire force range, basically from 0 pN to 400 pN, since the distributions were not bilateral symmetry. Indeed, in Chapter 2.1.3, it tells that $\tau(F)$, approximated by using Gaussian distribution, can be derived from the highly non-Gaussian rupture-force distribution, with a numerical coefficient differing by <10% [4][23].

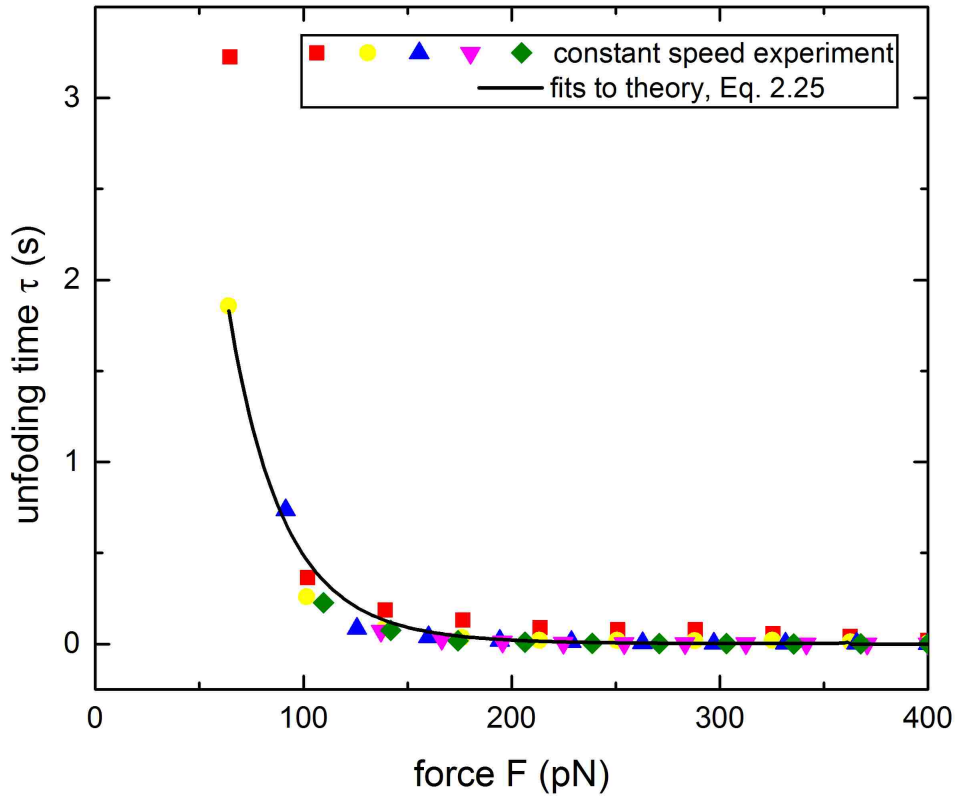

Figure 3.8: Lifetime $\tau(F)$ as a function of the applied force F, obtained by transforming the unfolding force histograms in Figure 3.7 according to Eq. (2.32) (filled colored symbols). The data are only for pulling polyprotein $(GB1)_8$ in PBS buffer with 0M GdmCl and 30% Glycerol. Different colored symbols correspond to different constant pulling speeds v. The black line is obtained by least squares fit to the colored symbols with Eq. (2.25), setting the scaling factor $\nu = 2/3$ (linear-cubic surface).

Figure 3.9 shows more detailed fitting results of the (lifetime, force) pairs by transforming the unfolding force histograms in Figure 3.7 according to Eq. (2.32), as well as applying Eq. (2.33) to get the relationship between the lifetime at the mean unfolding force and the variance of the unfolding-force distribution. Eq. (2.33):

$$\tau(\langle F\rangle) \approx \left[\frac{\pi}{2}(\langle F^2\rangle - \langle F\rangle^2)\right]^{1/2} / \dot{F}(\langle F\rangle)$$

For the later approach, only one pair of $(\langle F\rangle, \tau(\langle F\rangle))$ can be extracted from one constant-speed experiment thereby rendering more pulling speeds are required for fitting to Eq. (2.25). From Figure 3.9, we can see that, for each buffer solution, both (lifetime, force) pairs still collapse onto one single master curve, indicating that both the two approaches are available to use. The black solid lines are obtained by plotting least squares fit to the data points to Eq. (2.25), with scaling factor $\nu = 2/3$, corresponding to a linear-cubic energy landscape profile. To understand the fitting results better, we also tried fitting the data points with the scaling factor $\nu = 1$ and

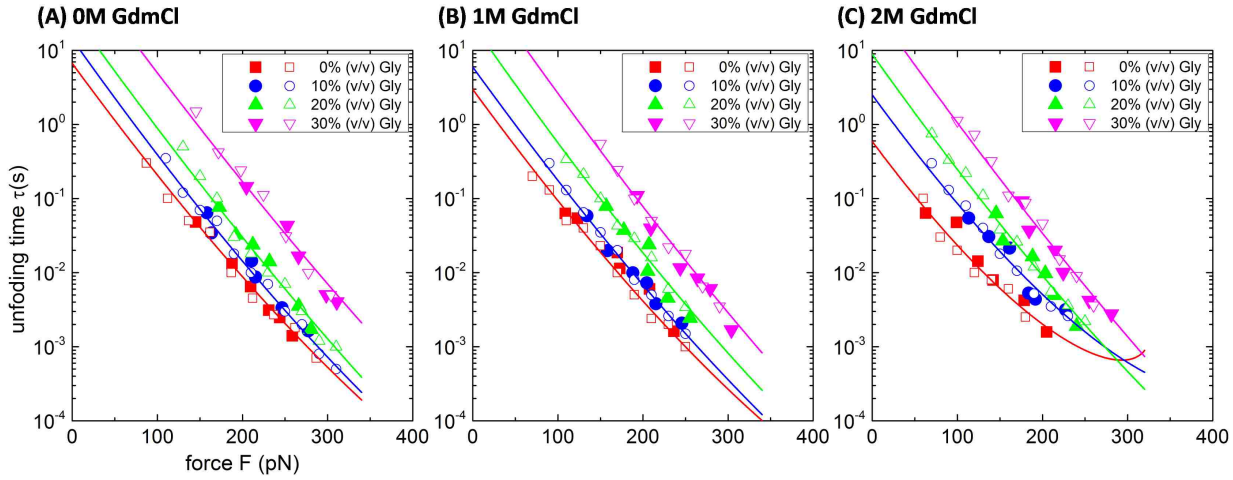

Figure 3.9: Lifetime $\tau(F)$ as a function of the applied force F for different concentrations of GdmCl and various concentrations of glycerol. All open symbols are obtained by transforming the unfolding force histograms in Figure 3.7 according to Eq. (2.32), while all filled symbols show the results from the mean and variance of the unfolding force distributions according to Eq. (2.33). The black lines are obtained by least squares fit to the symbols with Eq. (2.25), setting the scaling factor $\nu = 2/3$ (linear-cubic surface). Meanwhile, we also fit the data with $\nu = 1$ and $1/2$ (the cusp surface), shown in Table 3.2.

$\nu = 1/2$ (corresponding to the cusp surface introduced in Chapter 2.1.3). All the fitting results are shown in Table 3.2, and will be discussed afterwards.

3.3.1 Results

According to Table 3.2, we got several major conclusions of the mechanical properties of polyprotein $(GB1)_8$ by pulling it with AFM. As described in Chapter 2.2 about the experimental methods, we carried out the unfolding experiments of GB1 at different concentrations of GdmCl and various concentrations of Glycerol, to quantify the changes of mechanical stability and unfolding energy landscape resulting from the chemical denaturation and solvent viscosity.

The mechanical unfolding distance is unaltered by denaturant

The mechanical folding/unfolding process of proteins is determined by the energy landscape. The shape of the mechanical unfolding energy landscape is characterized by two important parameters, namely the barrier width $\Delta x^{\ddagger}$ and the barrier height ΔG. By adding the chemical denaturants, we were able to quantify the contribution of chemical denaturants.

Figure 3.10 shows the plot of the fitted distance $\Delta x^{\ddagger}$ between the native folded state and the transition state with free-energy surface factor $\nu = 2/3$ (similar results for $\nu = 1/2$ and 1) for different concentrations of GdmCl. Comparing the three curves, we saw that the value of $\Delta x^{\ddagger}$ is ~ 0.18 Å, with a small fluctuation around it. In the absence of chemical denaturant GdmCl, we obtained 1.75 ± 0.15 Å $\leq \Delta x^{\ddagger} \leq 1.86 \pm 0.22$ Å for various solvent viscosities ranging from ~ 0.86 mPa s to ~ 2.57 mPa s; for solution with 1M GdmCl, we obtained 1.84 ± 0.23 Å $\leq \Delta x^{\ddagger} \leq 1.85 \pm 0.20$ Å; and for solution with 2M GdmCl, we obtained 1.78 ± 0.15 Å $\leq \Delta x^{\ddagger} \leq 1.85 \pm 0.20$ Å. Actually, all the values of $\Delta x^{\ddagger}$ are within 1.8 ± 0.25 Å. Taking a look at the fitted values of $\Delta x^{\ddagger}$ in Table 3.2, we also found that, for each solvent condition of experiment, the barrier width $\Delta x^{\ddagger}$ usually decreased a little as the scaling factor ν increased from 1/2 to 1. However, the minimum value of $\Delta x^{\ddagger}$ in Table 3.2 is 1.58 ± 0.10 Å, while the maximum is 2.00 ± 0.35 Å, so it is still rather insensitive to the fitting scaling factor ν, which corresponds

to a specific free-energy surface. Actually, our results agree with these obtained by other groups before, which reported that $\Delta x^{\ddagger}$ is $\sim$ 1.7 Å to $\sim$ 2.0 Å [12][50]. Therefore, we concluded that, the denaturant GdmCl has minimal influence on the mechanical unfolding distance.

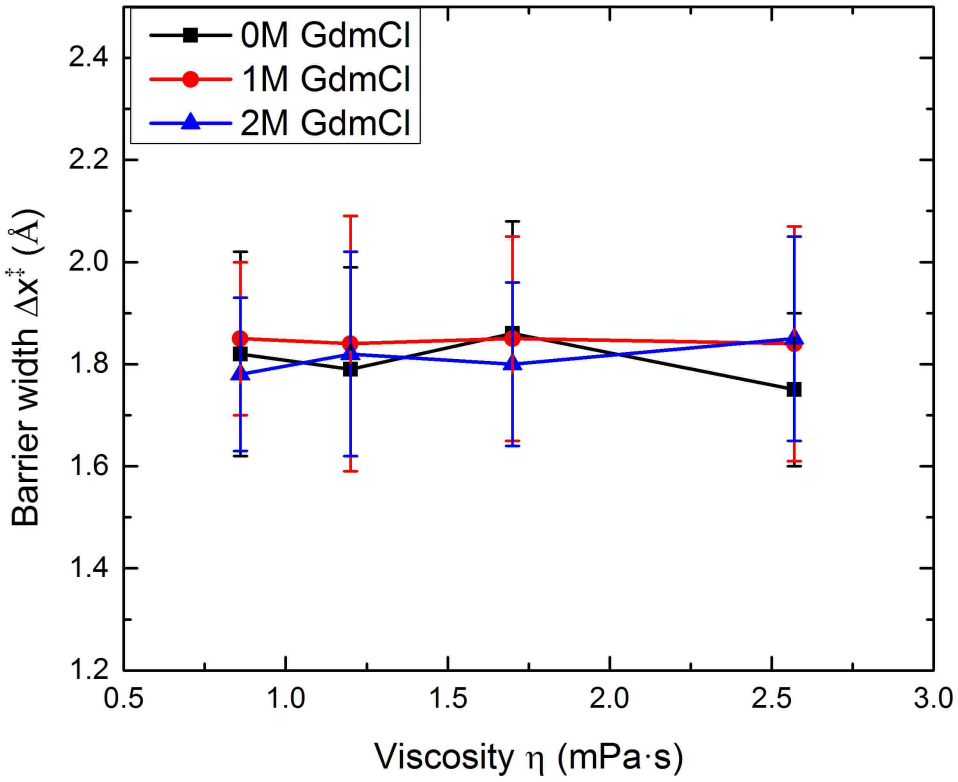

Figure 3.10: The distance between the folded state and the transition state. The unfolding distance $\Delta x^{\ddagger}$ of GB1 is plotted versus the solvent viscosity η. The filled symbols represent the data from Table 3.2 by least squares fit to Dudko's model with Eq. (2.25), with the surface factor $\nu = 2/3$ (similar results for $\nu = 1$ and $1/2$). The value of $\Delta x^{\ddagger}$ is $\sim$ 1.8 Å with a small fluctuation for different concentrations (0M, 1M, and 2M) of denaturant GdmCl in various viscosities of solution (0% glycerol, 10% glycerol, 20% glycerol, and 30% glycerol).

Meanwhile, it is also demonstrated that changing the viscosity of the experimental solution by adding different concentrations of glycerol didn't alter the distance between the native folded state and the transition state. The change of solvent viscosity allowed us to quantify the internal friction in single molecular experiments.

Chemical denaturants decrease the free-energy barrier height

In the previous section, we concluded that the presence of chemical denaturation (GdmCl) has minimal influence on the location of the transition state along the reaction coordinate, which is one of the two parameters related to the shape of the unfolding energy landscape. According to Dudko's model, we extracted the other parameter, the free-energy barrier height ΔG by least squares fit of Eq. (2.25) to the collapsed (unfolding time, force) pairs as shown in Figure 3.8.

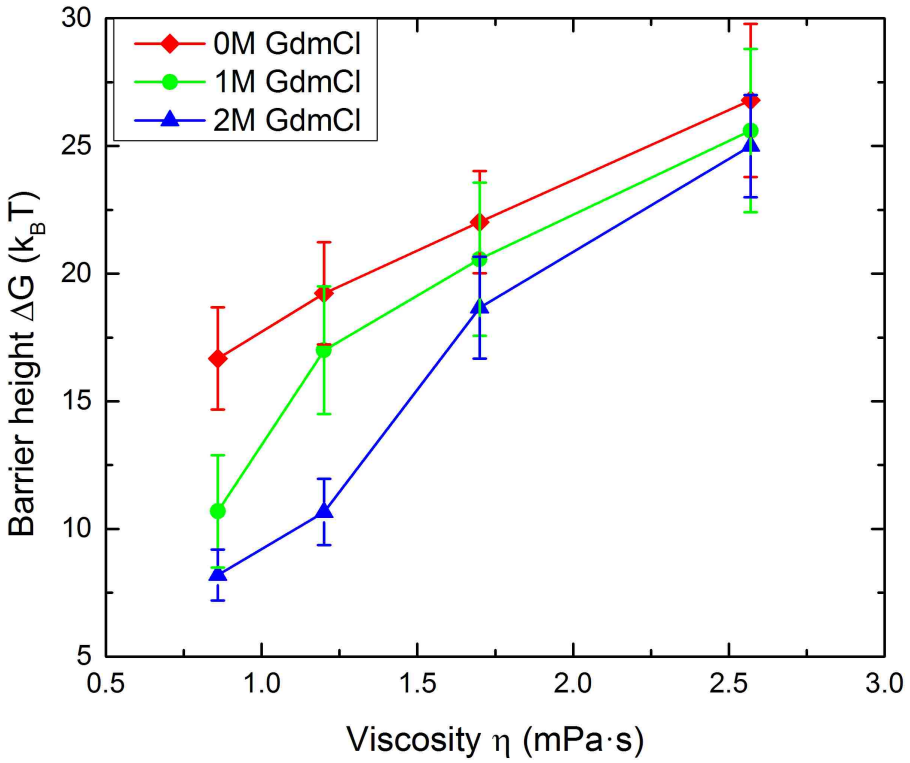

Figure 3.11: The free-energy barrier height for mechanical unfolding of GB1. The unfolding barrier height ΔG of GB1 is plotted versus the solvent viscosity η. The filled symbols represent the data from Table 3.2 by least squares fit to Dudko's model with Eq. (2.25), with the scaling factor $\nu = 2/3$. In the presence of denaturant GdmCl, the activation energy required for the polyprotein to unfold decreased (from red curve to blue curve). For pure PBS (0% glycerol), $\Delta G = 16.7 \pm 2.0$ k_BT; for PBS at 2M GdmCl (0% glycerol), $\Delta G = 8.2 \pm 1.0$ k_BT.

The plot of extracted energy barrier height for different concentrations of denaturant GdmCl is shown in Figure 3.11. We realized that, for PBS solution without any denaturant GdmCl, the free energy barrier height ΔG is the highest; as the concentration of GdmCl increased from 0M to 2M, the height of the barrier decreased from 16.7 ± 2.0 k_BT to 8.2 ± 1.0 k_BT for pure

PBS solution, assuming a linear-cubic energy surface profile ($\nu = 2/3$). For $\nu = 1$ and $1/2$, similar phenomenon was observed. Therefore, based on the fitting results of Dudko's model, we concluded that the denaturation GdmCl can decrease the barrier height, and make it easier to activate the polyprotein $(GB1)_8$ to unfold.

Note that in the presence of glycerol, the height of the barrier increased as the solvent viscosity increased.

Chemical denaturants speed up the mechanical unfolding process

The previous two sections show how the mechanical unfolding energy landscape was influenced by the chemical denaturant GdmCl and glycerol. The fact that the location of the transition state at different GdmCl concentrations remains unchanged suggests that the denaturation GdmCl does not alter the mechanical unfolding pathway for GB1. However, the height of the barrier decreases in the presence of GdmCl, compared with that in pure PBS. Therefore, it predicts a higher intrinsic unfolding rate for the protein in a solution with GdmCl. To confirm this prediction, we extracted the intrinsic unfolding rate/lifetime with Dudko's model.

Figure 3.12 shows the plot of intrinsic lifetime versus the solvent viscosity at different concentrations of GdmCl, fit to Dudko's model with Eq. (2.25), with the scaling factor $\nu = 2/3$. It is evident that the intrinsic lifetimes of GB1 decreased with the increase of GdmCl concentration. For pure PBS (0M GdmCl, 0% glycerol), the intrinsic lifetime $\tau_0 \sim 6.8$ s, while for PBS at 2M GdmCl (0% glycerol), $\tau_0 \sim 0.58$ s. The spontaneous unfolding rate increased from ~ 0.15 s^{-1} in pure PBS to ~ 1.71 s^{-1} in 2M GdmCl (0% glycerol). These results were also true for scaling factor $\nu = 1$ and $1/2$.

Glycerol slows down the mechanical unfolding process

We have talked about the denaturant GdmCl's effects on the unfolding process of GB1, and concluded that the distance between the native folded state and the transition state along the reaction coordinate is not affected by the solvent viscosity. However, considering the trend of the

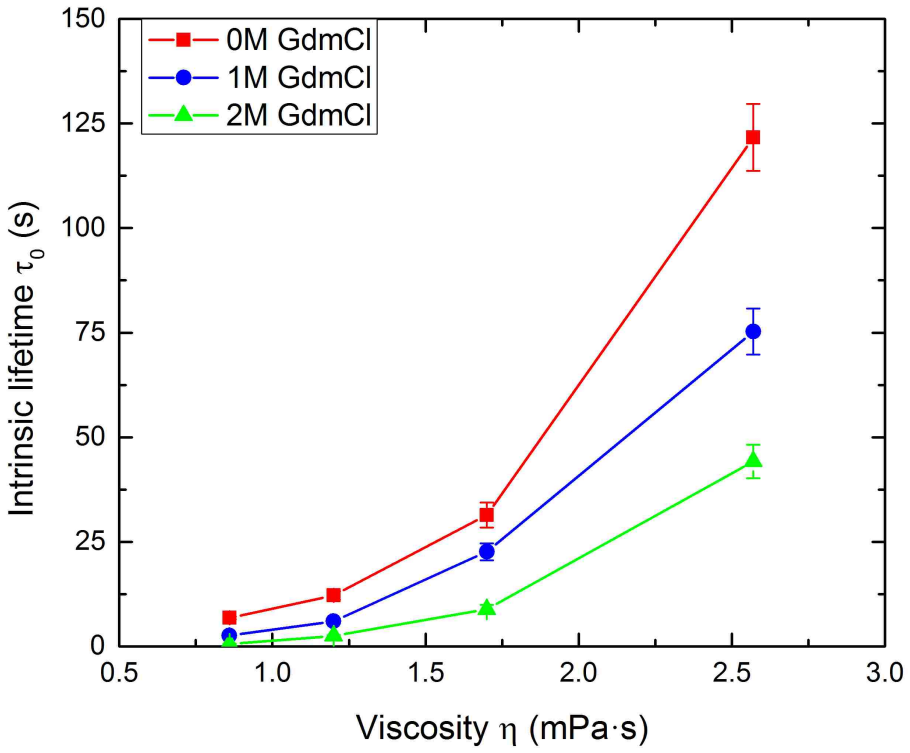

Figure 3.12: Intrinsic lifetime as a function of solvent viscosity at different denaturant concentrations. The intrinsic lifetime τ_0 of GB1 is plotted versus the solvent viscosity η. The filled symbols represent the data from Table 3.2 by least squares fit to Dudko's model with Eq. (2.25), with the scaling factor $\nu = 2/3$. The intrinsic lifetime of GB1 decreases with the increase of GdmCl concentration, from ~ 6.8 s in in PBS (0M GdmCl, 0% glycerol) to ~ 0.58 s in PBS (2M GdmCl, 0% glycerol). These results are also true for scaling factor $\nu = 1$ and $1/2$. The unfolding rate constant $k_0 = \tau_0^{-1}$ of GB1 increases with the increase of GdmCl concentration.

barrier height curves for each concentration of GdmCl in Figure 3.11, we found that the barrier height at the transition state is positively correlated with the solvent viscosity. As a consequence, it is predicted that the spontaneous unfolding rate constant should decrease with the increase of solvent viscosity. To confirm this prediction, we turned to Figure 3.12. The data is from Table 3.2 by least squares fit to Dudko's model with Eq. (2.25), with the scaling factor $\nu = 2/3$. The intrinsic lifetime τ_0 of GB1 did increase with the increase of solvent viscosity, from 6.8 ± 0.3 s in pure PBS (0% glycerol, 0M GdmCl) to 121.7 ± 8.0 s in PBS (30% glycerol, 0M GdmCl). These results were also true for other concentrations of GdmCl (1M and 2M) and for different scaling factors ($\nu = 1$ and $1/2$). The spontaneous unfolding rate constant $k_0 (= \tau_0^{-1})$ decreased as the solvent viscosity increased, indicating that a higher solvent viscosity causes the mechanical

unfolding process to slow down. Note that the intrinsic lifetime increased *nonlinearly* with the increase of the solvent viscosity, which is related to the next chapter about the internal friction.

η (mPa s)	ν	0M GdmCl			1M GdmCl			2M GdmCl		
		τ_0 (s)	$\Delta x^\ddagger$ (Å)	ΔG (k_BT)	τ_0 (s)	$\Delta x^\ddagger$ (Å)	ΔG (k_BT)	τ_0 (s)	$\Delta x^\ddagger$ (Å)	ΔG (k_BT)
0.86	1/2	8.2 ± 0.4	1.89 ± 0.20	18.4 ± 2.0	2.97 ± 0.20	1.88 ± 0.20	12.8 ± 2.5	0.65 ± 0.03	1.91 ± 0.20	9.2 ± 1.7
	2/3	6.8 ± 0.3	1.82 ± 0.20	16.7 ± 2.0	2.58 ± 0.20	1.85 ± 0.15	10.7 ± 2.2	0.58 ± 0.03	1.78 ± 0.15	8.2 ± 1.0
	1	4.2 ± 0.3	1.60 ± 0.10	—	1.98 ± 0.13	1.58 ± 0.10	—	0.49 ± 0.02	1.63 ± 0.10	—
1.20	1/2	18.1 ± 1.0	1.91 ± 0.20	23.1 ± 3.0	7.72 ± 0.30	1.92 ± 0.30	19.3 ± 2.5	2.78 ± 0.20	1.90 ± 0.22	15.1 ± 1.6
	2/3	12.2 ± 1.0	1.79 ± 0.20	19.2 ± 2.0	5.99 ± 0.50	1.84 ± 0.25	17.0 ± 2.5	2.50 ± 0.20	1.82 ± 0.20	10.7 ± 1.3
	1	7.7 ± 0.5	1.64 ± 0.10	—	4.67 ± 0.30	1.63 ± 0.10	—	1.61 ± 0.10	1.61 ± 0.10	—
1.70	1/2	38.8 ± 2.5	1.94 ± 0.24	26.2 ± 3.5	24.3 ± 2.5	1.98 ± 0.30	25.3 ± 3.0	11.8 ± 1.0	1.95 ± 0.27	23.8 ± 2.5
	2/3	31.4 ± 3.0	1.86 ± 0.22	22.0 ± 2.0	22.6 ± 2.0	1.85 ± 0.20	20.6 ± 3.0	8.9 ± 1.0	1.80 ± 0.16	18.7 ± 2.0
	1	22.7 ± 2.0	1.65 ± 0.12	—	14.4 ± 1.0	1.66 ± 0.12	—	6.4 ± 0.4	1.60 ± 0.10	—
2.57	1/2	157.0 ± 8.0	1.88 ± 0.24	30.9 ± 4.0	126.3 ± 9.5	1.91 ± 0.30	30.0 ± 5.0	61.7 ± 5.5	2.00 ± 0.35	29.3 ± 4.5
	2/3	121.7 ± 8.0	1.75 ± 0.15	26.8 ± 3.0	75.3 ± 5.5	1.84 ± 0.23	25.6 ± 3.2	44.2 ± 4.0	1.85 ± 0.20	25.2 ± 2.0
	1	67.1 ± 5.0	1.69 ± 0.12	—	55.7 ± 3.5	1.71 ± 0.10	—	38.6 ± 4.0	1.62 ± 0.12	—

Table 3.2: Extracted mechanical parameters for unfolding of protein GB1 obtained by least squares fit to Dudko's model with Eq. (2.25). The scaling factor $\nu = 1/2$ and $2/3$ correspond to the cusp and linear-cubic free-energy surfaces, respectively. For $\nu = 1$, and for $\Delta G \to \infty$ independent of ν, it corresponds to the phenomenological result. The datasets used to fit are obtained by transforming the unfolding force histograms of stretching polyprotein $(GB1)_8$ at different concentrations of denaturant GdmCl (0M, 1M, and 2M) and various concentrations of glycerol (0%, 10%, 20%, and 30%), according to Eq. (2.32).

Chapter 4

Internal friction

According to Kramers two-state theory at strong friction limit, the escape rate is derived as

$$k = \frac{\omega_0 \omega_b}{2\pi\gamma} \exp(-\beta E_b)$$

where ω_0 and ω_b denote the angular frequencies, E_b is the barrier height, γ is the overall friction, and $\beta = (k_B T)^{-1}$ is the thermal factor. As described in Chapter 2.3, the overall friction accounts for all the mechanisms that the energy can dissipate out during the reaction process. **The second goal of our study** is to quantify the internal friction directly from the extracted kinetic parameters according to Bell-Evans model or Dudko's model. To realize this, we develop an extended Ansari-expression, Eq. (2.45)

$$\tau_0 = k_0^{-1} = C(\sigma + \eta)^d$$

where τ_0 and k_0 denote the intrinsic lifetime and the spontaneous unfolding rate, respectively; C and d are the adjustable parameters; η and σ represent the solvent friction (i.e., viscosity) and internal friction, respectively.

We have already extracted the spontaneous unfolding rate k_0 at different solvent viscosities η for different denaturant concentrations (0M, 1M, and 2M) by both Bell-Evans model and Dudko's model in Chapter 3, then we performed least squares fit to Eq. (2.45).

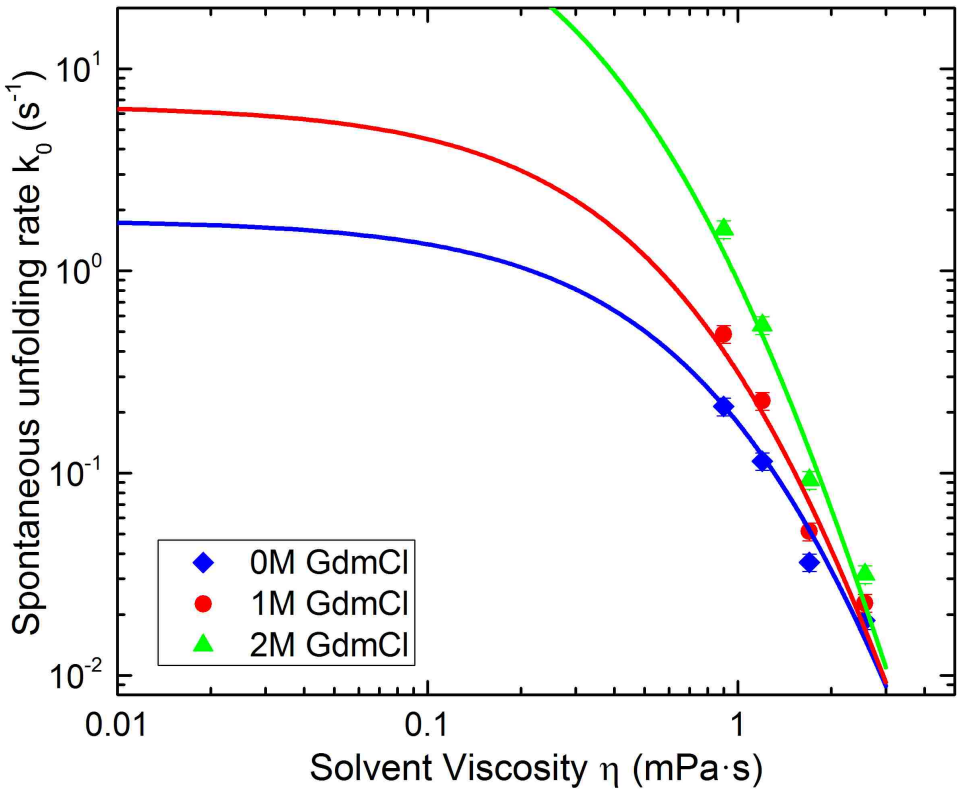

Figure 4.1: Spontaneous unfolding rate k_0 as a function of solvent viscosity η. The spontaneous unfolding rate k_0 of GB1 in different concentrations of denaturant GdmCl (0M, 1M, and 2M) is plotted versus the solvent viscosity η. The filled symbols represent the unfolding rate k_0 extracted according to Bell-Evans model (Chapter 3.2). Colored solid lines represent the best fits of spontaneous unfolding rate to the extended Ansari-expression (Eq. (2.45)), developed by us. For 0M GdmCl, it leads to $\sigma = 2.22 \pm 0.21$ mPa s, $C = 250 \pm 48$ mPa, and $d = 6.3 \pm 0.2$; for 2M GdmCl, it leads to $\sigma = 0.85 \pm 0.13$ mPa s, $C = 98 \pm 15$ mPa, and $d = 6.0 \pm 0.4$. More fitting results are shown in Table 4.1.

Figure 4.1 shows the best fit of the spontaneous unfolding rate k_0 of GB1 unfolding process, which was extracted according to Bell-Evans model (Chapter 3.2). For 0M GdmCl, it leads to $\sigma = 2.22 \pm 0.21$ mPa s, $C = 250 \pm 48$ mPa, and $d = 6.3 \pm 0.2$; for 2M GdmCl, it leads to $\sigma = 0.85 \pm 0.13$ mPa s, $C = 98 \pm 15$ mPa, and $d = 6.0 \pm 0.4$. Table 4.1 gives the detailed fitting results of the internal friction σ, the coefficient C, and the power index d, which were fitted to the extended Ansari-expression (Eq. (2.45)). The spontaneous unfolding rate k_0 was obtained in Chapter 3, according to both Bell-Evans model and Dudko's model (free-energy surface factor ν = 1/2, 2/3, and 1).

Comparing the fitting results with spontaneous unfolding rate extracted from both Dudko's model and Bell-Evans model, we realized that the values of internal friction σ, for each concentration of GdmCl, agree with each other quite well, while some deviation for the value of coefficient C. One important finding is that, the internal friction is *reduced* by the denaturant GdmCl, from ~ 2.1 mPa s without any denaturant to ~ 1.0 mPa s with 2M denaturant GdmCl. The decrease of internal friction probably plays an important role in accelerating GB1 unfolding process, due to the presence of denaturant GdmCl. The other important finding is that, the power index d remains nearly unchanged/insensitive ($d \sim 6.5$) even with the presence of denaturation. This result suggests that the power index d might be a characteristic constant in GB1 and other proteins's folding/unfolding dynamics. To further validate this prediction, more experimental and theoretic work is needed.

	0M GdmCl			1M GdmCl			2M GdmCl		
Dudko's	σ (mPa s)	C (mPa)	d	σ (mPa s)	C (mPa)	d	σ (mPa s)	C (mPa)	d
$\nu = 1/2$	2.07 ± 0.30	160.4 ± 32	6.4 ± 0.5	1.40 ± 0.25	123.5 ± 20	6.6 ± 0.8	0.86 ± 0.15	105.8 ± 15	6.4 ± 0.7
$\nu = 2/3$	2.09 ± 0.20	203.7 ± 38	6.6 ± 0.6	1.73 ± 0.22	190.7 ± 30	6.5 ± 0.6	1.12 ± 0.11	120.7 ± 19	6.7 ± 0.6
$\nu = 1$	2.17 ± 0.12	239.0 ± 45	6.5 ± 0.4	1.85 ± 0.21	220.0 ± 38	6.5 ± 0.2	0.96 ± 0.30	209 ± 28	6.3 ± 0.2
Bell-Evans	2.22 ± 0.21	250 ± 48	6.3 ± 0.2	1.55 ± 0.18	185 ± 24	6.2 ± 0.3	0.85 ± 0.13	98 ± 15	6.0 ± 0.4

Table 4.1: Internal friction at different concentrations of denaturation GdmCl. The parameters, i.e., internal friction σ, the coefficient C, and the power index d, were fitted to the extended Ansari-expression (Eq. (2.45)). The spontaneous unfolding rate k_0 was obtained in Chapter 3, according to both Bell-Evans model and Dudko's model (with free-energy surface factor ν = 1/2, 2/3, and 1). The internal friction is *reduced* by the denaturant GdmCl, from ~ 2.1 mPa s without any denaturant to ~ 1.0 mPa s with 2M denaturant GdmCl, which probably plays an important role in GB1 unfolding process.

Chapter 5

Conclusion

Single-molecule atomic force microscopy (AFM) experiments have been carried out with a home-built AFM. Combining the AFM experiments and the models derived from Kramers theory (Bell-Evans model and Dudko's model), we have obtained protein mechanical stabilities at a single molecule level.

By changing the solvent viscosity and the concentrations of denaturant GdmCl, we validated that the chemical denaturant speeds up the mechanical unfolding process of the protein GB1. Denaturant decreases the height of free-energy barrier at the transition state, but has minimal influence on the distance between the native unfolded state and the transition state.

We successfully quantified the internal friction in the unfolding of GB1 protein by using an extended form of Ansari-expression. By fitting the extracted mechanical properties to the expression, we found that the internal friction decreases from ~ 2.1 mPa s without any denaturant to ~ 1.0 mPa s with 2M denaturant GdmCl. The decrease of internal friction probably plays an important role in accelerating GB1 unfolding process. This procedure provides new insights into how internal friction affects protein folding/unfolding, with potential implication in protein folding diseases such as Alzheimer's, Parkinson's and Huntington's diseases.

Bibliography

[1] H. A. Kramers. Brownian motion in a field of force and the diffusion model of chemical reactions. *Physica*, 7(4):284–304, 1940.

[2] G. I. Bell. Models for the specific adhesion of cells to cells. *Science*, 200(4342):618–627, 1978.

[3] E. Evans and K. Ritchie. Dynamic strength of molecular adhesion bonds. *Biophysical Journal*, 72(4):1541–1555, 1997.

[4] O. K. Dudko, G. Hummer, and A. Szabo. Intrinsic rates and activation free energies from single-molecule pulling experiments. *Physical Review Letters*, 96(10), 2006.

[5] K. C. Neuman and A. Nagy. Single-molecule force spectroscopy: optical tweezers, magnetic tweezers and atomic force microscopy. *Nature Methods*, 5(6):491–505, 2008.

[6] D. Aioanei, S. Lv, I. Tessari, et al. Single-molecule-level evidence for the osmophobic effect. *Angewandte Chemie-International Edition*, 50(19):4394–4397, 2011.

[7] D. Beece, L. Eisenstein, H. Frauenfelder, et al. Solvent viscosity and protein dynamics. *Biochemistry*, 19(23):5147–5157, 1980.

[8] A. Ansari, C. M. Jones, E. R. Henry, et al. The role of solvent viscosity in the dynamics of protein conformational-changes. *Science*, 256(5065):1796–1798, 1992.

[9] S. J. Hagen. Solvent viscosity and friction in protein folding dynamics. *Current Protein & Peptide Science*, 11(5):385–395, 2010.

[10] A. Soranno, B. Buchli, D. Nettels, et al. Quantifying internal friction in unfolded and intrinsically disordered proteins with single-molecule spectroscopy. *Proceedings of the National Academy of Sciences of the United States of America*, 109(44):17800–17806, 2012.

[11] Y. Cao and H. B. Li. Polyprotein of gb1 is an ideal artificial elastomeric protein. *Nature Materials*, 6(2):109–114, 2007.

[12] Y. Cao and H. B. Li. How do chemical denaturants affect the mechanical folding and unfolding of proteins? *Journal of Molecular Biology*, 375(1):316–324, 2008.

[13] P. Hanggi, P. Talkner, and M. Borkovec. Reaction-rate theory: fifty years after kramers. *Reviews of Modern Physics*, 62(2):251–341, 1990.

[14] G. E. Uhlenbeck and L. S. Ornstein. On the theory of the brownian motion. *Physical Review*, 36(5):823–841, 1930.

[15] S. N. Zhurkov. Kinetic concept of the strength of solids. *Int. J. Fract. Mech.*, 1(4):311–322, 1965.

[16] S. Arrhenius. Über die reaktionsgeschwindigkeit bei der inversion von rohrzucker durch säuren. *Z. Phys. Chem. Lpz.*, 4:226, 1889.

[17] C. Gergely, J.-C. Voegel, P. Schaaf, et al. Unbinding process of adsorbed proteins under external stress studied by atomic force microscopy spectroscopy. *Proceedings of the National Academy of Sciences of the United States of America*, 97(20):10802–10807, 2000.

[18] D. A. Simson, M. Strigl, M. Hohenadl, and R. Merkel. Statistical breakage of single protein a-igg bonds reveals crossover from spontaneous to force-induced bond dissociation. *Phys. Rev. Lett.*, 83:652–655, 1999.

[19] A. Garg. Escape-field distribution for escape from a metastable potential well subject to a steadily increasing bias field. *Physical Review B*, 51(21):15592–15595, 1995.

[20] G. Hummer and A. Szabo. Kinetics from nonequilibrium single-molecule pulling experiments. *Biophysical Journal*, 85(1):5–15, 2003.

[21] C. Friedsam, A. K Wehle, F. Kuhner, et al. Dynamic single-molecule force spectroscopy: bond rupture analysis with variable spacer length. *Journal of Physics-Condensed Matter*, 15(18):S1709–S1723, 2003.

[22] C. Ray, J. R. Brown, and B. B. Akhremitchev. Rupture force analysis and the associated systematic errors in force spectroscopy by afm. *Langmuir*, 23(11):6076–6083, 2007.

[23] O. K. Dudko, G. Hummer, and A. Szabo. Theory, analysis, and interpretation of single-molecule force spectroscopy experiments. *Proceedings of the National Academy of Sciences of the United States of America*, 105(41):15755–15760, 2008.

[24] M. Raible, M. Evstigneev, P. Reimann, et al. Theoretical analysis of dynamic force spectroscopy experiments on ligand-receptor complexes. *J Biotechnol*, 112(1-2):13–23, 2004.

[25] M. Abramowitz and I. A. Stegun. *Handbook of Mathematical Functions*. Oxford, New York, 2003.

[26] M. Rubinstein and R. H. Colby. *Polymer physics*. Oxford University, Oxford; New York, 2006.

[27] S. B. Smith, Y. Cui, and C. Bustamante. Overstretching b-dna: the elastic response of individual double-stranded and single-stranded dna molecules. *Science*, 271(5250):795–9, 1996.

[28] Theo Odijk. Stiff chains and filaments under tension. *Macromolecules*, 28(20):7016–7018, 1995.

[29] M. D. Wang, H. Yin, R. Landick, et al. Stretching dna with optical tweezers. *Biophysical Journal*, 72(3):1335–1346, 1997.

[30] P. Gross, N. Laurens, L. B. Oddershede, et al. Quantifying how dna stretches, melts and changes twist under tension. *Nat Phys*, 7(9):731–736, 2011.

[31] C. Bustamante, J. F. Marko, E. D. Siggia, et al. Entropic elasticity of lambda-phage dna. *Science*, 265(5178):1599–1600, 1994.

[32] J. F. Marko and E. D. Siggia. Stretching dna. *Macromolecules*, 28(26):8759–8770, 1995.

[33] J. Gore, Z. Bryant, M. Nollmann, et al. Dna overwinds when stretched. *Nature*, 442(7104):836–839, 2006.

[34] T. Lionnet, S. Joubaud, R. Lavery, et al. Wringing out dna. *Physical Review Letters*, 96(17):178102, 2006.

[35] Maxim Y. Sheinin and Michelle D. Wang. Twist-stretch coupling and phase transition during dna supercoiling. *Physical Chemistry Chemical Physics*, 11(24):4800–4803, 2009.

[36] E. L. Florin, M. Rief, H. Lehmann, et al. Sensing specific molecular-interactions with the atomic-force microscope. *Biosensors & Bioelectronics*, 10(9-10):895–901, 1995.

[37] B. Zagrovic and V. Pande. Solvent viscosity dependence of the folding rate of a small protein: Distributed computing study. *Journal of Computational Chemistry*, 24(12):1432–1436, 2003.

[38] P. G. de Gennes. *Scaling Concepts in Polymer Physics*. Cornell University Press, New York, 1979.

[39] A. M. Gronenborn, D. R. Filpula, N. Z. Essig, et al. A novel, highly stable fold of the immunoglobulin binding domain of streptococcal protein g. *Science*, 253(5020):657–661, 1991.

[40] U. Sjobring, L. Bjorck, and W. Kastern. Streptococcal protein-g - gene structure and protein-binding properties. *Journal of Biological Chemistry*, 266(1):399–405, 1991.

[41] P. Alexander, J. Orban, and P. Bryan. Kinetic analysis of folding and unfolding the 56 amino acid igg-binding domain of streptococcal protein g. *Biochemistry*, 31(32):7243–8, 1992.

[42] P. Alexander, S. Fahnestock, T. Lee, et al. Thermodynamic analysis of the folding of the streptococcal protein g igg-binding domains b1 and b2: why small proteins tend to have high denaturation temperatures. *Biochemistry*, 31(14):3597–603, 1992.

[43] S. H. Park, M. C. Shastry, and H. Roder. Folding dynamics of the b1 domain of protein g explored by ultrarapid mixing. *Nat Struct Biol*, 6(10):943–7, 1999.

[44] E. L. McCallister, E. Alm, and D. Baker. Critical role of beta-hairpin formation in protein g folding. *Nat Struct Biol*, 7(8):669–73, 2000.

[45] B. A. Krantz, L. Mayne, J. Rumbley, et al. Fast and slow intermediate accumulation and the initial barrier mechanism in protein folding. *J Mol Biol*, 324(2):359–71, 2002.

[46] M. Carrion-Vazquez, A. F. Oberhauser, S. B. Fowler, et al. Mechanical and chemical unfolding of a single protein: A comparison. *Proceedings of the National Academy of Sciences of the United States of America*, 96(7):3694–3699, 1999.

[47] M. Schlierf and M. Rief. Temperature softening of a protein in single-molecule experiments. *Journal of Molecular Biology*, 354(2):497–503, 2005.

[48] H. Dietz, F. Berkemeier, M. Bertz, et al. Anisotropic deformation response of single protein molecules. *Proceedings of the National Academy of Sciences of the United States of America*, 103(34):12724–12728, 2006.

[49] X. H. Zhang, S. E. Craig, H. Kirby, et al. Molecular basis for the dynamic strength of the integrin $\alpha 4\beta 1$/vcam-1 interaction. *Biophysical Journal*, 87(5):3470–3478, 2004.

[50] T. Shen, Y. Cao, S. Zhuang, et al. Engineered bi-histidine metal chelation sites map the structure of the mechanical unfolding transition state of an elastomeric protein domain gb1. *Biophys J*, 103(4):807–16, 2012.

Biography

Wei Zhang was born in March 12, 1989 in Hefei, China. In 2007, he was admitted by University of Science and Technology of China (USTC), and then got the Bachelor of Science degree in Physics four years later. He has a strong interest in fields of mathematics, physics, as well as biology.

In 2009, Wei, together with another three students from the Department of Chemistry, proposed a project as *the Surface Modification of Nanometer Fe_3O_4 and its Application* and was rewarded the third prize in the 5th competition of physical Research Experiments of University. Later he joined Lab of Laser-Biology at USTC, where his thesis was finished. Under the supervision of Prof. Yinmei Li, Wei completed the project, *Optical Tweezers to Study the Non-specific Binding between the Polystyrene Spheres and the Cells*. During the undergraduate study at USTC, Wei won Outstanding Freshman Scholarship (11/2007), and Outstanding Student Scholarship (11/2009). In the summer of 2009, he taught Mathematics for senior high school students.

From August, 2011, Wei acts as a PhD student, supervised by Prof. Xiaohui (Frank) Zhang at Lehigh University. His research focuses on the mechanical kinetics in single molecular field, with atomic force microscopy (AFM) and optical tweezers technique. In particular, he and postdoc Yizhen Wang just completed the research about the mechanical properties of elastic polyprotein $(GB1)_8$ with home-build AFM, and are preparing for the publication. During the first two years at Lehigh University, he was awarded Dean's Doctoral Student Assistantship (09/2011) and Fellowship of Lehigh University (09/2012). He is looking forward to getting more experience in single molecular field and working on his PhD project from Prof. Zhang.